2013

Yield Detection for Non-Destructive Testing using Ultrasonic Signal Processing

Bharath Murali Thekkedath
Louisiana State University and Agricultural and Mechanical College

YIELD DETECTION FOR NON-DESTRUCTIVE TESTING USING ULTRASONIC SIGNAL PROCESSING

A Thesis

Submitted to the Graduate Faculty of the
Louisiana State University and
Agricultural and Mechanical College
in partial fulfillment of the
requirements for the degree of
Master of Science in Electrical Engineering

in

The Department of Electrical and Computer Engineering

by
Bharath Murali Thekkedath
Bachelor of Engineering, Anna University, 2008
May 2013

ACKNOWLEDGEMNETS

First and foremost, I would like to thank my thesis advisor and major professor Dr. Hsiao-Chun Wu for his patient and precious supervision. His guidance, knowledge, and support for this research project were the key to the completion of this work. I am very grateful to him for leading me to this wonderful and promising signal processing area and demonstrating the brilliant scientific perception. I would also like to express my sincere gratitude to Dr. Ayman Okeil in the Department of Civil and Environmental Engineering at Louisiana State University (LSU) for exposing me to the field of non-destructive testing (NDT)--a popular structural health monitoring tool and providing the invaluable data for this study. I am greatly thankful to his former student, Dr. Yilmaz Bingol, from whom I developed the essential background for NDT research and explored the scientific depth in this field. I would also like to thank Dr. Bahadir Gunturk for teaching me pattern recognition and statistical techniques in machine learning and participating in my thesis committee.

Besides, I am very thankful to Dr. Matt Fannin at the Department of Agricultural Economics and Agribusiness of LSU for having been supporting me financially for nearly two years.

I greatly appreciate my lab mate Ms. Hongting Zhang for her valuable time and effort in providing crucial inputs and suggestions for this thesis.

I am very thankful to my sister's family for their love and support.

At last but not least, I would like to thank my parents for their unwavering support and all my friends here at LSU for making my academic life very memorable.

TABLE OF CONTENTS

LIST OF TABLES

LIST OF FIGURES

NOMENCLATURE

SHM:	Structural Health Monitoring
NDT:	Non-Destructive Testing
LDA:	Linear Discriminant Analysis
ROC:	Receiver Operating Characteristics

ABSTRACT

Structural health monitoring (SHM) is a very important field for many engineering disciplines. SHM deals with the monitoring of material structures periodically for assessing the lifetimes of the structures. There are various techniques for SHM. Non-destructive testing (NDT) is one of the most popular SHM tools to monitor structures. It demonstrates the indispensable advantage of providing structural health assessment without the need of intrusion. In this thesis, a new NDT tool for yield detection using ultrasonic signal processing is investigated.

In this work, for the study of yield detection, steel specimen samples have been acquired, which were obtained from the laboratory of Department of Civil and Environmental engineering at Louisiana State University (LSU). An ultrasonic transducer then collected the signal data when these samples were tested. The data were preprocessed and segmented. For each acquired ultrasonic signal waveform, a total of three dominant echoes were extracted for the yield detection. A total of nine different signal features were extracted from these echoes for each ultrasonic signal. These nine features include time-domain features (signal amplitude, signal energy) and transform-domain features (wavelets, discrete Fourier transform, chirp Z-transform, discrete cosine transform, and discrete sine transform). Based on these aforementioned features, the linear discriminant analysis (LDA) technique is proposed to classify two situations (no-yield and yield). The proposed LDA-based classifier is compared with the conventional classifiers using individual features. The classifiers' performances are evaluated using the receiver operating characteristics (ROC) plots.

According to our experiments, it is discovered that the LDA-based classifier for yield detection is superior to all conventional classifiers using individual features, in terms of high detection rates subject to the fixed false detection rates.

CHAPTER 1: INTRODUCTION

This chapter provides the overview of *structural health monitoring* (SHM). A crucial SHM approach, namely *non-destructive testing* (NDT), together with its applications will be introduced here. Subsequently, digital signal processing methods for NDT applications will also be presented.

1.1 Structural Health Monitoring (SHM)

Structural health monitoring is a very important field as it poses direct impacts on our daily life. According to [1], structural health monitoring is defined as a process where damage identification strategies for various mechanical, civil, and aerospace infrastructures are implemented to monitor the quality of the structures or the materials. *Damage* is defined as any change induced in the system (due to aging, fatigue, or external force), which causes long-lasting effects on the infrastructures [1]. Many structures are being continually used despite their aging and wear resulting in the accumulation of damages and a potential cause of danger. Therefore, people had better monitor the structures for their safety.

Structural health monitoring has long been researched and studied. During the 19^{th} century, a technique using hammer sound was invented where the sound from striking was investigated to determine if any internal damage existed in the material structure [1]. In recent years, people have shown a vast interest in SHM technologies due to the awareness of public safety [1]. Generally speaking, structural health monitoring is carried out in the way that a structure or a system is observed in a periodic manner where damage-related features are extracted from the periodically acquired measurements and then a statistical analysis is

conducted to assess the damage status of the structure or the system. The primary goal of SHM is to characterize the material properties and identify defects and deficiencies in the structures.

There are various techniques in use to monitor the status of the structure during its lifetime. These techniques range from the conventional mechanisms such as visual test to the modern scientific approaches involving complex embedded systems, which help to attain high accuracy and robustness.

The structural health condition can be monitored using the systems connected with optical sensors and wireless transceivers [2] to collect data about the structure. This is feasible during the construction phase of the structure. Nevertheless, the existing structures that have already been constructed also need to be evaluated regarding its lifetime as the ill-condition might jeopardize lives (such as bridges, dams, reactors, etc.). Structural health monitoring has a wide range of applications. It has been used in different industries including semiconductor manufacturing [1], aerospace-vehicle/aircraft manufacturing/maintenance, building construction, railroad monitoring, etc.

1.2 Non-Destructive Testing (NDT)

Non-destructive testing (NDT) or *non-destructive evaluation and testing* (NDE&T) is a kind of SHM technique/tool. NDT relies on the interdisciplinary efforts (see [3]), which assures the integrity of the structural components and systems so that they can perform in an economical and efficient way.

NDT involves various tools and methodologies for inspecting and assessing the condition of a structure/system without intrusion so as to retain their future usefulness [3]. Thus NDT can perform SHM without causing any damage to the material structures or systems. Non-destructive

testing has been broadly used in assessing many modern structures such as bridges, dams, pipelines, aircrafts, and other complex structures due to the aforementioned advantage. There are various classical NDT techniques addressed in literature such as the *tap test* and the *visual inspection* (*visual test*). In the former technique, the material is inspected by people who tap on it and listen to the sound changes indicating defects in the material; in the latter technique, the material is inspected visually so that the cracks and the dislocations in the material can be identified by experts. These classical tests, obviously, cannot explore the internal failures within the structures/systems. This deficiency in early NDT techniques was later overcome with the help of rapid advancements in computer technologies, embedded hardware, and scientific growth in various engineering disciplines. Disciplines including computer science and engineering, digital signal processing, telecommunications, etc. enable the development of new robust and efficient NDT techniques and methodologies. The commonly-used NDT methods include

- Liquid Penetrant Test
- Magnetic Particle Test
- Microwave/Ground Penetrating Radar
- Eddy Current Testing
- Radiography (X-Ray/Gamma Ray)
- Impact-Echo Method
- Acoustic Emission
- Visual/Optical Method
- Sonic/Resonance
- Ultrasonic Inspection.

In this thesis study, we focus on NDT using ultrasonic signal processing (or ultrasonic inspection). The overviews on NDT using digital signal processing and the ultrasonic inspection will be presented in Sections 1.3 and 1.4. In Chapter 2, the detailed description of our method and the corresponding experiment setup will be provided.

1.3 Digital Signal Processing in NDT

Digital signal processing (DSP) has improved and advanced the state-of-the-art of NDE&T techniques [4]. The increasing demands and expectations of industries involved in productivity and safety have triggered new technologies such as robotics, computer design, and instrumentation and led to automation. Thus, one can perceive the extensive use of NDT in automated defect detection and characterization nowadays. Signal processing has played a pivotal role for NDT in making it an automated and a reliable structural health monitoring tool/technique by providing it with granular inspection, reliable decision-making, and discriminative information.

In recent years, much research emphasis has been made on the development of the new procedures and processes that enhance the reliability of the conventional NDT techniques. Thus The advanced signal processing concepts which have already been used in other applications such as sonar, radar, etc. are being adopted for NDT [4]. DSP is an engineering field that involves acquiring signal data and transforming the obtained data into useful information/features by digital means. A simple block diagram of signal processing and its application for NDT is illustrated in Figure 1.

As depicted in Figure 1, a signal processing system involves *signal acquisition*, *signal enhancement*, and *signal information retrieval*.

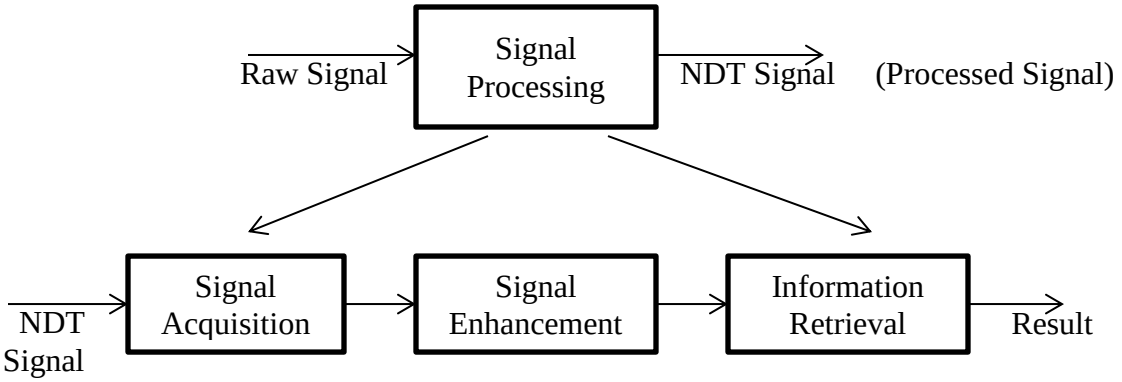

Figure 1. NDT signal processing (duplicate from [4]).

DSP has been widely used in various engineering fields/industries including medical imaging (electrocardiogram or ECG, ultrasound scan, etc.), navigation technologies such as radar and sonar, telecommunications, pattern recognition, and NDE&T, etc.

The general objectives of employing DSP in NDT include but are not limited to (see [4]):

- Improving reliability in inspection
- Improving defect detection accuracy
- Improving defect classification accuracy
- Developing new NDT tools to characterize material properties
- Monitoring structural processes such as welding, cutting, grinding, etc.

DSP can also be used to automate data acquisition and data analysis and thus greatly reduce the chance for any occurrence of human error during the process. Fundamental DSP techniques such as averaging, filtering, and other signal enhancement schemes have shown phenomenal improvements in system detection capabilities. With the help of DSP, the detailed defect information can be explored and assessed to prolong or accurately predict a structure's lifetime. The crucial information includes the *type*, *shape*, and *size* of the flaws/defects in the structures. Conventional DSP tools such as *discrete Fourier transform* (DFT) and *discrete wavelet*

transform (DWT) have been widely used for investigating signals. The ultrasonic wave velocity was estimated using the *fast Fourier transform* (FFT) (efficient implementation of DFT) [5].

On the other hand, DWT has also been employed for the NDT applications in the past few decades. Some advantages of DWT over DFT/FFT include its superior time-frequency localization property and adaptability to different signal characteristics.

In summary, DSP has been playing a pivotal role in the NDT for structural health assessment. Therefore, we focus on the advanced DSP techniques for NDT in this thesis work. Among various DSP methodologies for NDT, we will investigate the ultrasonic signal processing based NDT or *ultrasonic NDT*. In the next section, the introduction of ultrasonic inspection will be provided.

1.4 Ultrasonic NDT (Ultrasonic Inspection)

Ultrasonic inspection is one of the most popular NDT methods. The ultrasonic testing technology uses high-frequency sound signal called *ultrasound*. The basic principle of ultrasonic testing is that an ultrasound is transmitted to the material being inspected and the multiple back surface echoes are reflected from the material defects or the fault locations. Ultrasonic inspection has been broadly used for testing a variety of materials including metals, ceramics, and polymers [6]. Ultrasonic signal processing techniques are employed therein to detect the defects confined in materials, which include cracks, voids, and other structural deficiencies [7]. The signal processing techniques enabling ultrasonic inspection have also assisted in finding the material properties (ex. modulus and strength) [8].

An illustration of ultrasonic testing for material characterization in practice is shown in Figure 2.

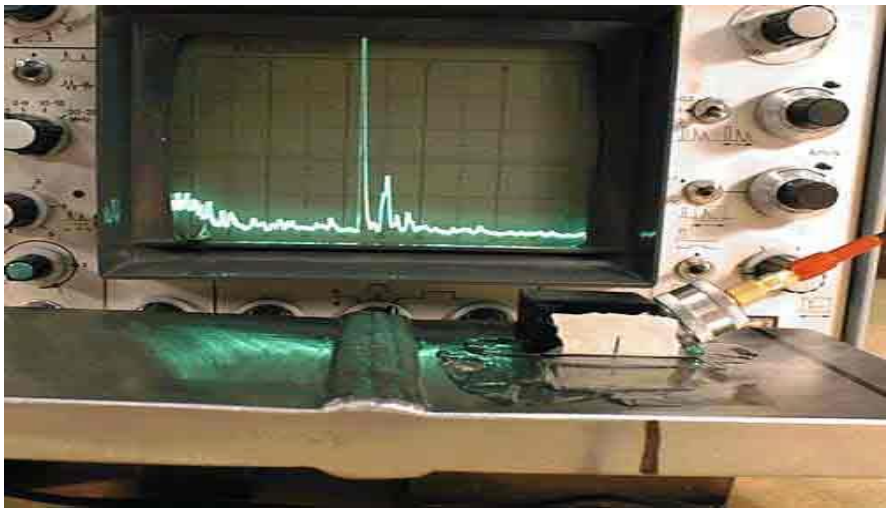

Figure 2. Ultrasonic testing illustration (this picture was acquired from [3] and the written permission to use this picture here has been authorized).

The details of ultrasonic signal processing and its applications for NDT will be discussed in Chapter 2.

1.5 Applications of Non-Destructive Testing (NDT)

NDT is often used if the material/structure/system being tested needs to be evaluated without damaging the specimen/structure under test. NDT has many practical applications, which involve industrial activities such as automotive, aviation/aerospace, civil/construction engineering, and petroleum/chemical production, etc. As most industries require the constant evaluation on the facility safety and the reliability of the structures/systems, NDT plays a major role in providing the necessary monitoring techniques/tools. Some modern NDT applications used by manufacturers include (see [8]):

- Ensuring product integrity and reliability
- Avoiding failures and saving human lives from accidents occurring
- Ensuring customers' satisfaction and manufacturer's reputation
- Facilitating better product design

- Maintaining operational readiness
- Controlling manufacturing process
- Lowering manufacturing costs
- Maintaining uniform quality level

1.6 Thesis Outline

This thesis is mainly focused on the yield detection using signal features and transforms. A comparative study is conducted to find a reliable yield detection technique. A *linear discriminant analysis* (LDA) based yield detection technique is proposed in this study and the performances of different classifiers are compared.

The rest of this thesis is organized as follows. Chapter 2 presents a brief discussion on the ultrasonic NDT in SHM. It also provides some insights into the experimental setup used in this study for obtaining the test signals for yield detection. In Chapter 3, how to extract various signal features in the time-domain and transform-domain and the LDA based classification technique are both discussed in detail. In Chapter 4, a thorough comparative study is made for the yield detection techniques using the aforementioned ultrasonic signal features stated in Chapter 3. The performance in comparison is via the *receiver operating characteristics* (ROC) curves. Finally, conclusion will be drawn in Chapter 5.

CHAPTER 2: ULTRASONIC NON-DESTRUCTIVE EVALUATION AND TESTING

2.1 Ultrasonic Non-Destructive Testing for Structural health monitoring

Ultrasonic inspection (UI) techniques have been playing a vital role in the applications such as sound navigation and ranging (sonar). Meanwhile, they have also been utilized for medical diagnosis [9] as well as SHM. Ultrasound has been used to characterize submerged objects by sonar and to detect the moving objects inside a human body by medical instrumentation. NDT was early introduced during the World War II due to the prosperity in technological developments especially for military purposes. In early days, NDT was mostly used in detecting material defects [9]. Back then, new sophisticated techniques such as ultrasonic testing, eddy currents, x-rays, etc. were proposed to boost the effectiveness of NDT. Apart from detecting defects, NDT can often be used to quantify the material and mechanical properties.

Ultrasonic signal processing techniques are widely used in *quantitative non-destructive evaluation and testing* (QNDE&T). QNDE&T applications include determination of the mechanical and structural properties, the dimensionality measurement of various complex structures and materials, etc. Figure 3 below demonstrates an often-encountered example for monitoring the body development of a fetus using the Doppler ultrasound.

2.1.1 Basic Principles of Ultrasonic Inspection

Ultrasounds are signals, which oscillate at very high frequencies beyond the audible frequency range of human ears. A typical UI system is capable of generating and collecting this kind of signals. Therefore, it should have various functional units, namely a pulser/receiver, a transducer, and some display devices. The function of a pulser/receiver is to generate high-voltage electrical pulses. Then the transducer transforms these electrical pulses to high-frequency ultrasonic signals.

Figure 3. Monitoring the fetus development using Doppler ultrasound (this figure was duplicated from [9] and the permission to use this graph has been granted).

During the test, an ultrasonic signal propagates through the structure of the specimen; when there exists a discontinuity in its traveling path, part of the signal will be reflected back from the discontinuity and part of the signal will still proceed. The received signal is then collected by the transducer and displayed on the monitor screen. From the signal waveform displayed on the monitor, the information about the location, size, and other features of the discontinuities can be acquired. Thus, one may use UI to spot flaws, cracks, voids, inclusions, etc. inside any material [7]. Figure 4 illustrates a basic schematic diagram containing the functional units of a typical UI system.

Ultrasonic inspection is very popular and versatile among all NDT technologies. The advantages of UI can be found as follows (see [9]):

- It is quite sensitive to the surface and the subsurface discontinuities.
- The depth level for detecting flaws is much higher compared to other NDT methods.

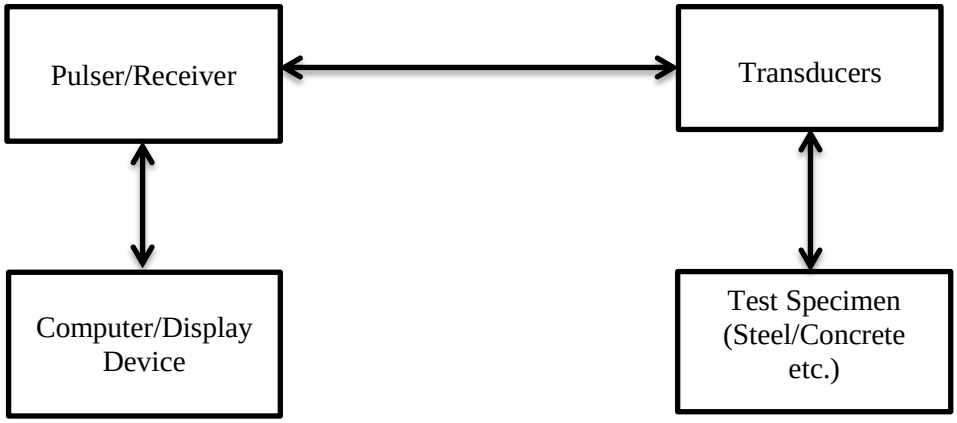

Figure 4. Block diagram of a typical ultrasonic testing system.

- During the test, the instrument needs to contact only a single side of the structure while maintaining very accurate test results.
- The advanced functional units can facilitate real-time evaluation and display.

On the other hand, UI has some limitations or drawbacks as follows:

- The internal surface being tested should be able to reflect ultrasonic signals.
- The structure (specimen) being tested cannot be irregular in shape, small, or rough.
- More skills are required for a UI operator compared to other NDT operators.

In general, UI has been broadly used for many applications in avionic/aerospace, spacecraft, and construction industries.

2.2 Ultrasonic NDT for Stress Analysis

In this thesis work, the experimental setup used for the stress analysis of steel was established by Professor Ayman Okeil and Dr. Yilmaz Bingol in the Department of Civil and Environmental Engineering of LSU. The UI facility consists of five major functional units [10]. They are

- An Ultrasonic Pulser/Receiver,

- Two Transducers,
- A PCI digitizer,
- A MTS Hydraulic Unit,
- A Personal Computer.

Figure 5 depicts the system diagram for this UI facility, where “P” indicates the test specimen, “A/D” means the analog-to-digital converter (PCI digitizer), “T/R” specifies the transmitting transducer, “R” specifies the receiving transducer, and “P/R” is the pulser and receiver. A brief description of the functional units in Figure 5 used for this study and the selected system parameters are provided in the subsequent context [10].

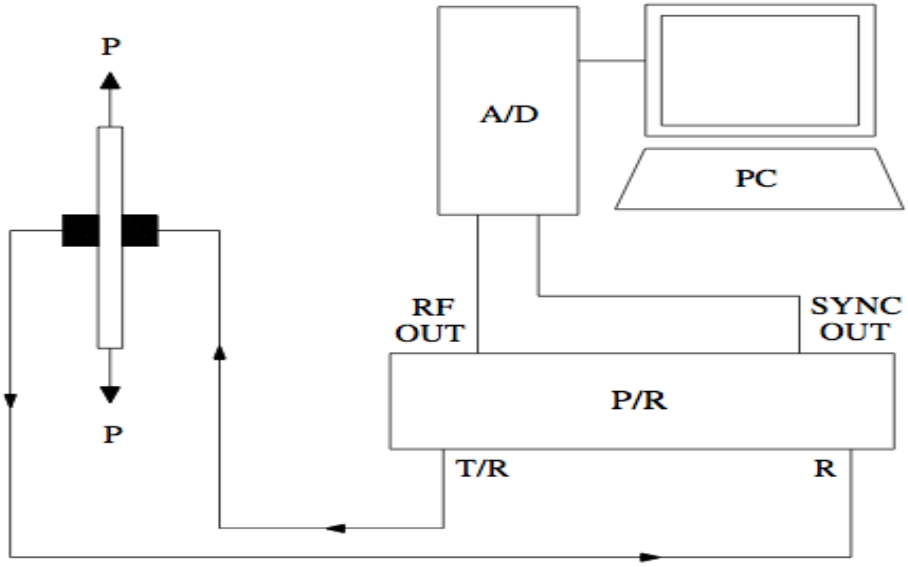

Figure 5. Experimental setup used for stress analysis [10].

2.2.1 Ultrasonic Pulser/Receiver

The ultrasonic pulser/receiver is the most important component in the UI system. It is critical to choose the appropriate operating frequency range. For the metals being tested in this

work, ultrasound with a high frequency greater than 1 MHz is used. Thus, a pulser/receiver, which can cover a wide frequency range, was adopted. A Panametrics Model 5900PR pulser/receiver was equipped with a maximum bandwidth of 1 kHz-200 MHz in the UI system as depicted in Figure 5.

2.2.2 Transducers

The ultrasonic transducers are also crucial components in the UI system. There are two types of waves that can be used for testing the specimens, namely the *longitudinal* and *shear* waves. Different ultrasonic transducers can be built upon the ways they generate the signals (ex., piezoelectric transducers, electromagnetic-acoustic transducer, etc.). In this thesis study, the piezoelectric transducers with both longitudinal- and shear-wave contacts are equipped. The transducers are connected to the pulser/receiver through a doubly shielded cable causing low cable noise and better performance. The transducers are placed on the test specimen with the help of a coupling medium. The coupling medium used in this study is an Ultragel II couplant from Sonotech Inc. [10].

2.2.3 PCI Digitizer

The main function of the PCI digitizer is to convert the analog signals obtained from the pulser/receiver to the digital domain. The sampling rate plays a critical role in data analysis. Generally speaking, the higher the sampling rate, the better resolution the discrete-time signal can demonstrate.

In this work, an Acqiris PCI digitizer Model DP310 was connected to the pulser/receiver and the computer. This digitizer has two operational modes, namely the *oscilloscope mode* and the *transient recorder mode*. The oscilloscope mode is a semi-automatic mode. The transient

recorder mode is a manual mode where the user has to prompt the sampling rate for the signal to be sampled.

2.2.4 MTS Hydraulic Unit

The hydraulic unit was used to apply desired stress on the tested specimen when the ultrasonic measurements were taken. In this work, the MTS 810 hydraulic unit was used and it was also connected to a personal computer where the user can specify the desired stress levels to be applied for testing the specimen.

2.2.5 Personal Computer

A personal computer was used to control the above-mentioned functional units. The output of the pulser/receiver is connected to the digitizer. The output of the digitizer is connected to the RS-232 serial port in the computer. The acquired signal samples are then stored so that various signal processing techniques can be employed.

2.3 Data Acquisition for Ultrasonic NDT

The signal data will be acquired using the experimental setup stated in Section 2.2. The ultrasonic data for stress analysis was acquired from the tested steel specimens. In this study, a total of four different steel specimens were considered, which possessed various thicknesses, mechanical properties, and chemical properties as listed in Table 1. We used the ultrasonic data obtained from the Type-I specimen for feature extraction.

Table 1. The properties of Type-I specimen

Specimen	Thickness	Mechanical Properties	
		Tensile Stress	Yield Stress
Type -I	¼ inches	63.1ksi	46.3ksi

The ultrasonic signals were obtained from the specimen via two ultrasonic test modes, namely *through transmission* (TT) and *pulse- echo* (PE) modes. A total of 183 ultrasonic signal waveforms were collected for the stress analysis from the Type-I specimen. The signal waveforms were sampled at the rate of 400 mega-samples/second. We fixed this sampling rate to collect all data.

Different stress levels were applied during the collection of the aforementioned signal data. These stress level conditions can be categorized into two groups, namely *no-yield stress levels* and *yield stress levels* as below. Note that the unit "ksi" means *kilo-pounds per square inch*.

Stress Levels Applied on the Steel Specimen

10ksi, 20ksi, 30ksi, 40ksi, 42.5ksi, 42ksi, 44ksi, 45ksi — No-Yield Stress Levels

47.5ksi, 48ksi, 50ksi, 52.5ksi, 55ksi, 57.5ksi, 60ksi, 62.5ksi, 62ksi, 65ksi, 67.5ksi, 68ksi

Yield Stress Levels

2.4 Yield Detection Using Ultrasonic Signal Processing

Ultrasonic signal processing has been playing a critical role in NDT applications. Stress analysis using ultrasonic signals has long been studied since the 1970's [11]. The employment of ultrasonic signals for stress analysis is based on the principle of *acousto-elasticity*, or *acoustoelastic effect*. The acousto-elasticity is described as the influence of the stress or strain states on the propagation velocities of the ultrasonic waves. This principle is similar to that of the

photoelasticity. Thus, the ultrasonic technology would allow use to monitor the state-of-the-art structures without impairing their integrity and functionality [12].

The application of acousto-elasticity helps to analyze the magnitude changes in the applied stresses on the tested materials using the velocity changes of the waves propagating through the tested materials. In recent years, ultrasonic NDT has been found vastly for the measurement of residual and applied stresses in materials such as wood, steel, and aluminum, etc.

In this thesis study, we adopt the ultrasonic signal processing to carry out the yield stress detection. In structural engineering, *yield* is a very important parameter for evaluating the structural strength and functionality. Yield is defined as a point where a structure loses its elastic property and tends to deform plastically. Thus, yield detection is a very important study in the structural health monitoring. Thus, analyzing the signal characteristics at various stress levels was presented in [13]. In this thesis, the ultrasonic signals obtained from the steel specimens at the pre- and post-yield states are investigated in the time- and transform-domains using advanced signal processing techniques. We also propose to integrate all existing signal features for yield detection, hopefully, to build an "optimal" framework in this work.

CHAPTER 3: AUTOMATIC FEATURE EXTRACTION FOR YIELD DETECTION

This chapter focuses on the ultrasonic signal processing for yield detection. The ultrasonic signal data samples will be segmented the signal features will be extracted for the yield analysis. The underlying signal features in the time domain and the transform domain will be manifested in detail. The concept of *linear discriminant analysis* (LDA) and its application for yield detection will be presented.

3.1 Automatic Feature Extraction for Ultrasonic Signals

The ultrasonic signals were obtained from the test specimen (steel) using the system as stated in Chapter 2. Each signal waveform was sampled at 400 MHz in a period of 20 μsec and hence the total number of samples was 8,000. Different stress levels were applied to generate different ultrasonic signals. Figure 6 illustrates a typical ultrasonic signal obtained from the test specimen when the applied stress is 10 *ksi* (**k**ilo-pounds per **s**quare **i**nch).

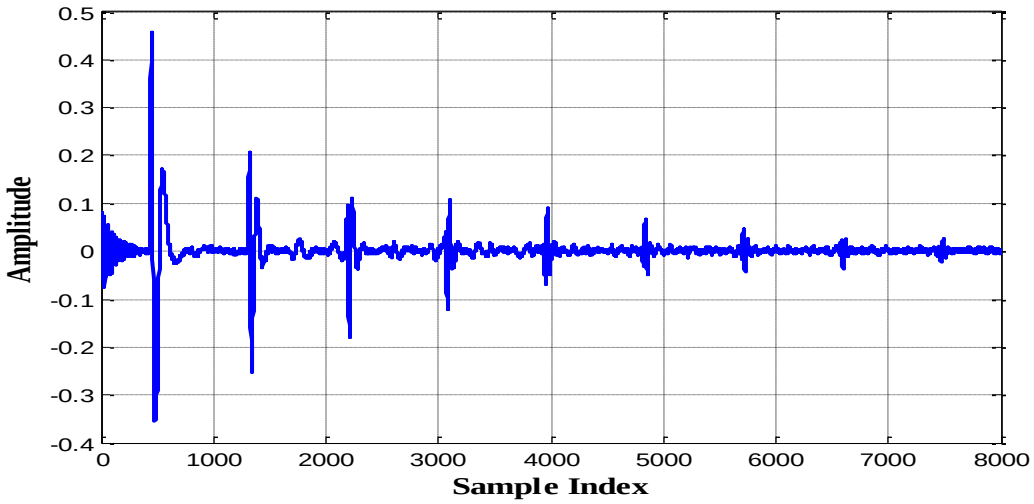

Figure 6. A typical ultrasonic signal waveform sampled at 400 MHz for 20 $\boldsymbol{\mu}$sec when 10 ksi of stress is applied on the test specimen.

In the previous work [10], the signal *echoes* (ex., dominant amplitudes in Figure 6) were manually extracted from the raw signals, which consist the commonly-believed essential features

for yield detection. Nevertheless, the manual operation would often draw human errors. Therefore, in this thesis study, the automatic segmentation technique is employed to obtain the signal echoes completely based on the computer algorithms. Once these echoes are spotted by the computer, the time- and transform-domain features can be readily extracted for the further signal analysis. Recently, our research group devised a new algorithm to *blindly* identify the echoes of the ultrasonic signals traveling within the composite materials [7]. We adopt this algorithm with modifications for the application of the echo identification in the ultrasonic signals obtained from the steel specimens during the yield analysis. With the employment of this algorithm, it can be found that each signal echo consists of a *starting point*, a *terminal point*, and a *peak*. Figure 7 depicts the results from the blind echo identification algorithm in [7] when the raw signal demonstrated in Figure 6 is used.

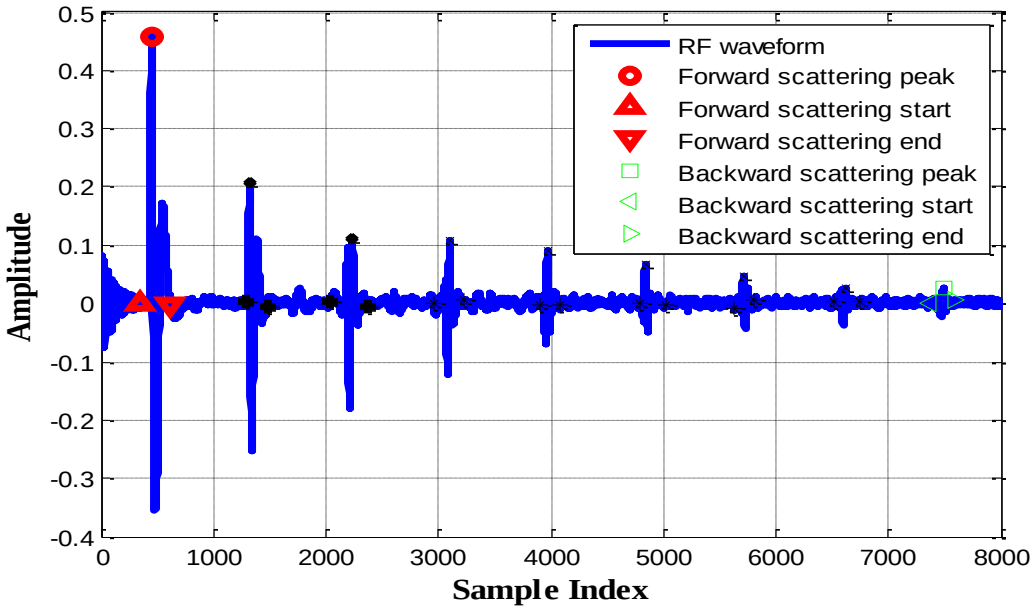

Figure 7. Determination of echoes with their starting points, terminal points, and peaks using the algorithm in [7]. The raw signal data is the same as used in Figure 6.

3.2 Signal Features Used for Ultrasonic NDT

For the yield analysis, one must discover the essential feature(s) to achieve the highest accuracy in evaluating the material properties. Although many preceding research works have paved quite some foundations, it is still an open problem. In this subsection, we will investigate some features in both time and frequency domain. It has been demonstrated that three dominant signal echoes could be used for effective and robust yield detection [13]. After the echoes are segmented, a moving-average filter can be applied for noise reduction. Then, features can be acquired from these filtered echoes.

3.2.1 Time-Domain Features

The first categories of features are time-domain features. These features are extracted directly from the signal time-series (raw waveforms). The time-domain features investigated in this thesis include

- Peak Amplitude
- Signal Energy

The details of the time-domain feature extraction are presented as follows.

3.2.1.1 Peak Amplitude

For a time-domain signal waveform, the *peak amplitude* is simply the maximum among all signal sample values. In the Figure 8 a signal echo is taken and the time domain signal amplitude is determined. For example, if $x(t)$ denotes a signal waveform, its peak amplitude is given by

$$\text{peak amplitude of } x(t) = max\ |x(t)|$$

Obviously, the peak amplitude is sensitive to any scaling factor. Hence, the extracted peak amplitudes should be normalized by both the first echo's peak amplitude obtained at the same stress level and the respective echo's amplitudes obtained from the zero-stress specimen [13].

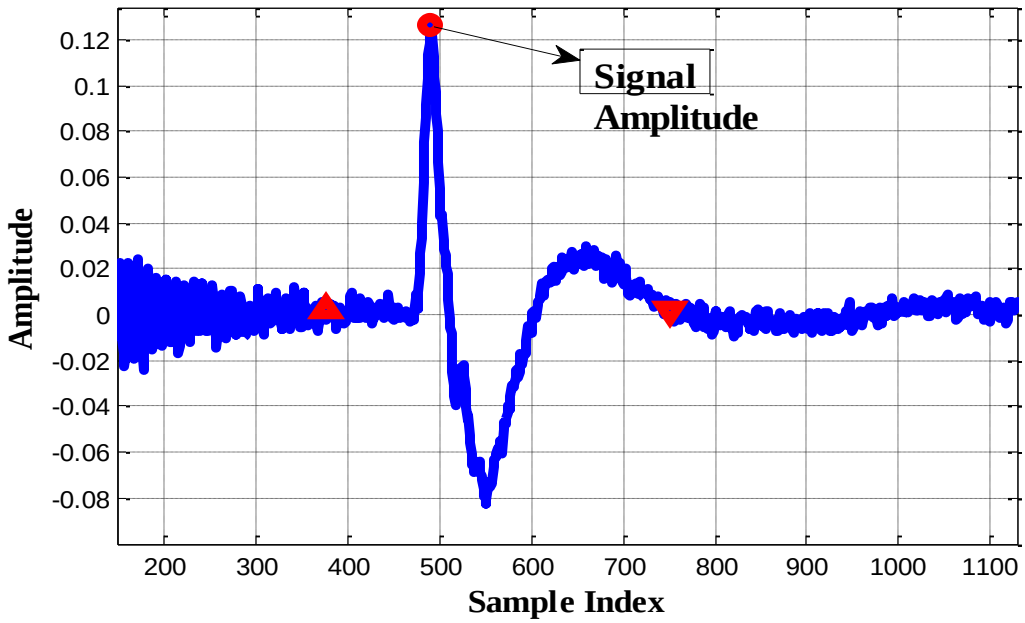

Figure 8. Illustration of the peak amplitude in a dominant ultrasonic echo.

3.2.1.2 Signal Energy

The signal energy of a signal is given as follows. For a discrete-time signal $x[i]$ with the sample size N, the *signal energy* is given by

$$\text{signal energy of } x[i] = \sum_{i=1}^{N} |x\,[i]|^2$$

Similar to the peak amplitude, the signal energy is quite sensitive to any scaling factor and hence it has to be normalized by the respective signal energy obtained from the zero-stress specimen [13].

3.2.2 Transform-Domain Features

One may apply any sort of transformation to transform the raw signal time-series to another domain, called *transform-domain*. Sometimes, the signal features are more useful when they are extracted from these transform-domains. The most popular transform for this use is surely the Fourier transform, which facilitates the spectral and frequency characteristics for any signal. Including the Fourier transform, we investigate a total of five transforms for the yield analysis in this thesis, namely *discrete wavelet transform* (DWT), *discrete Fourier transform* (DFT), *chirp-Z Transform* (CZT), *discrete cosine transform* (DCT), and *discrete sine transform* (DST). The discussion on these five transforms will be provided as follows.

3.2.2.1 Wavelet Transform

The continuous wavelet transform is a correlation between the signal and the wavelet basis functions. A *mother wavelet* $\varphi(t)$ is chosen and a set of *sub-wavelets* are constructed subject to a *dilation factor a* and a *translation factor b.* Thus the continuous wavelet coefficients of a continuous-time function $x(t)$ are given by

$$W_x(a,b) = \int_{-\infty}^{\infty} x(t)\varphi_{a,b}^{*}(t)\,dt,$$

where $\varphi_{a,b}(t)$ is defined as

$$\varphi_{a,b}(t) = \frac{1}{\sqrt{a}}\varphi\left(\frac{t-b}{a}\right)$$

and the superscript "*" denotes the conjugate operator. In order to obtain large values of correlation, the mother wavelet $\varphi(t)$ has to be chosen in such a way that it should match the shape of the signal. Thus, after the careful study of many wavelet families, bi-orthogonal 1.3 wavelet was chosen for the needed transform. Figure 9 illustrates the shape of the mother wavelet "bi-orthogonal 1.3".

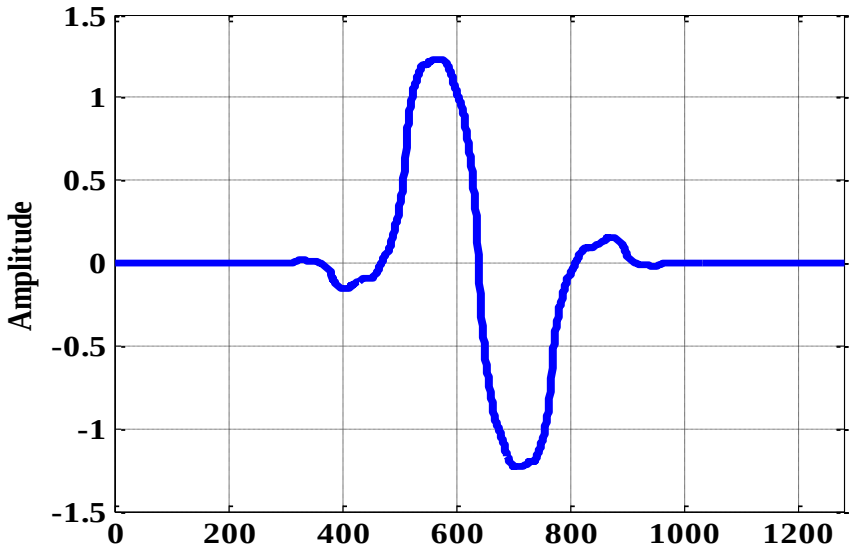

Figure 9. Bi-orthogonal 1.3 wavelet.

As the obtained ultrasonic signals are all discrete-time signals, the signals are decomposed using the *discrete wavelet transform* instead.

The discrete wavelet transform (DWT) is the transform facilitating the projections of a signal onto the underlying wavelet basis functions. The DWT framework consists of two main system blocks, namely *decomposition* and *reconstruction* blocks. In the decomposition phase, the discrete-time signal $x[n]$ is passed through a highpass filter represented by $H(z)$ (its transfer function) and then downsampled such that the obtained outcomes are called the *detail coefficients*. Meanwhile, the signal $x[n]$ is also passed through a lowpass filter represented by $L(z)$ and then downsampled such that the obtained outcomes are called the *approximate coefficients*. Actually, the approximate coefficients correspond to the *low-frequency high-scale components* of the signal whereas the detail coefficients are the *high-frequency and low-scale components* instead. Figure 10 shows the basic one-level DWT decomposition where $A_1(n)$ and $D_1(n)$ denote the approximate and detail coefficient sequences, respectively and the subscript "1" denotes the level index.

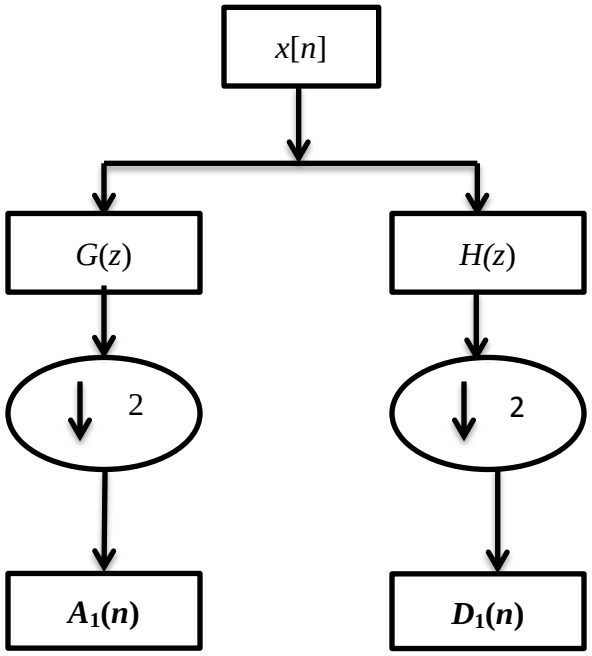

Figure 10. Illustration of one-level DWT decomposition.

The features extracted from the wavelet transform in this thesis are obtained through the three-level DWT decomposition. The three signal features extracted from the three-level decomposition are *wavelet peak amplitude*, *wavelet peak-to-peak amplitude*, and *wavelet root mean square* (*RMS*) *amplitude*. This three-level signal decomposition is illustrated in Figure 11. In Figure 11, $A_1(n)$ and $D_1(n)$ are the level-one approximate and detail coefficients resulting from the signal $x[n]$ convolved with the lowpass and highpass filters, respectively.

Then the level-one approximate coefficients are convolved with a lowpass filter and a highpass filter again; then $A_2(n)$ and $D_2(n)$ are the level-two approximate and detail coefficients, respectively. Similarly the level-two approximate coefficients are convolved with a lowpass filter and a highpass filter such that $A_3(n)$ and $D_3(n)$ are obtained as the level-three approximate and detail coefficients of the signal.

The DWT of a signal $x[n]$ is calculated by passing the samples through a series of filters.

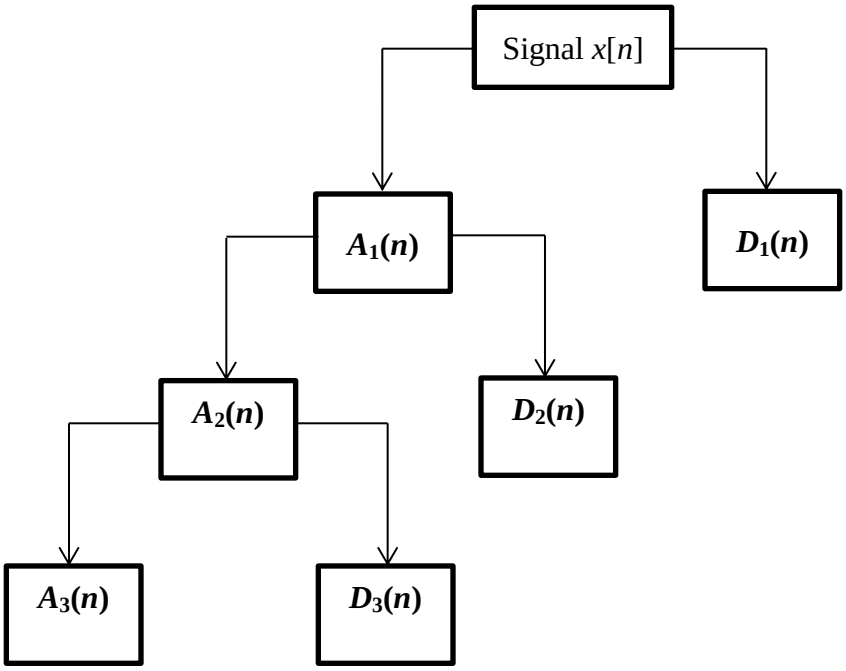

Figure 11. Illustration of the three-level DWT decomposition of a signal $x[n]$.

For a one-level DWT, the signal $x[n]$ is convolved with a lowpass filter and the output is given by

$$A_1(n) = x[n] * g[n] = \sum_{k=-\infty}^{\infty} x[k]g[n-k],$$

where $g[n]$ is the impulse response of lowpass filter. Meanwhile, the signal $x[n]$ is also convolved with a highpass filter resulting in the following output sequence:

$$D_1(n) = \sum_{k=-\infty}^{\infty} x[k]h[n-k],$$

where $h[n]$ is the impulse response of the highpass filter.

As half of the signal spectrum is removed, thus half of the signal samples can be removed according to *Nyquist's rule*. Thus, the outputs after downsampling by a factor of 2 are given by

$$A_1(n) = \sum_{k=-\infty}^{\infty} x[k]g[2n-k],$$

$$D_1(n) = \sum_{k=-\infty}^{\infty} x[k]h[2n-k].$$

For a three-level decomposition, the output coefficients are obtained after performing the convolution on the signal with the lowpass and the highpass filters once and then on the respective approximate coefficients two more times.

The following features are extracted from the ultrasonic signal echoes using the wavelet transform.

- Wavelet Peak Amplitude

When the level-three approximate coefficients $A_3(n)$ are obtained, the peak amplitudes of the wavelet approximate coefficients are calculated for all the signal echoes acquired from each stress level during the yield detection analysis. Figure 12 shows the maximum peak amplitude as calculated from the approximate coefficients $A_3(n)$ for a signal echo.

- Wavelet Peak-to-Peak Amplitude

We also calculate the wavelet peak-to-peak amplitudes from the approximate coefficients $A_3(n)$ as the essential features. The wavelet peak-to-peak amplitude is defined as the distance between the positive peak and the negative peak of the level-three approximate coefficients $A_3(n)$.

- Wavelet Root-Mean-Square (RMS) Amplitude

In addition, we also use the wavelet RMS amplitudes as the features. The RMS amplitude is defined as the square root of the sample mean of $A_3^2[n]$. The RMS value for a discrete sequence $x[n]$ is given by

$$\text{RMS (of a discrete sequence } x[n]) = \sqrt{\frac{1}{n}\sum_{i=1}^{n} x_i^2},$$

where n is the number of samples of the signal $x[n]$.

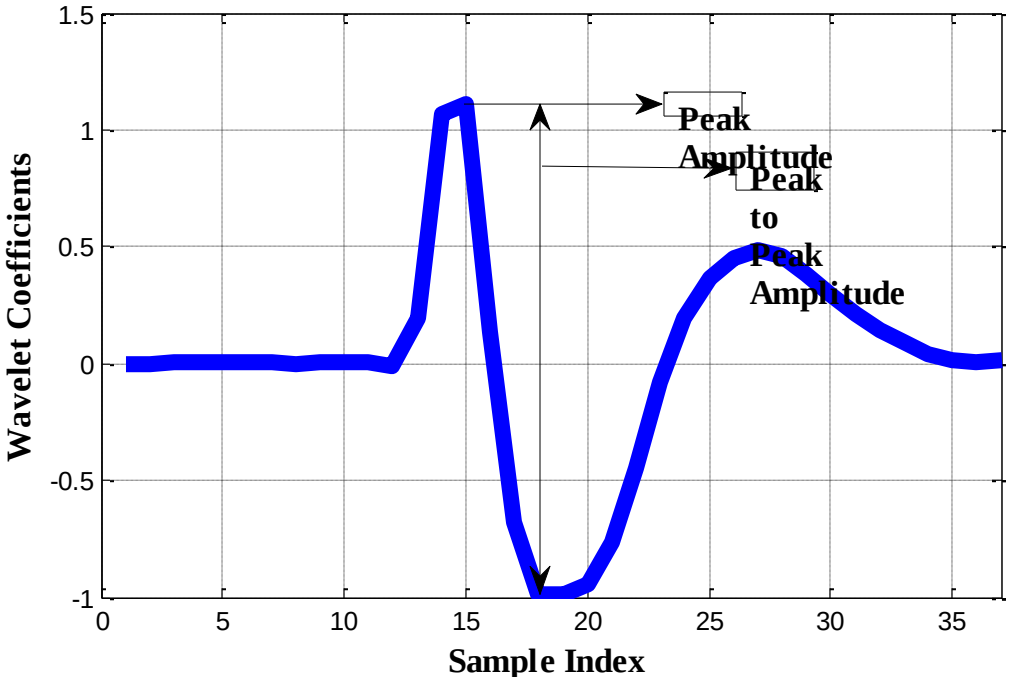

Figure 12. Wavelet peak amplitude and peak-to-peak amplitude.

Similar to the time-domain features, the wavelet transform features are quite sensitive to any scaling factor and hence it has to be normalized by the respective feature(s) obtained from the zero-stress specimen [13].

3.2.2.2 Discrete Fourier Transform (DFT)

We may use the discrete Fourier transform (DFT) peak amplitudes as the features for the yield analysis as well. In reality the DFT can be efficiently computed using the fast Fourier transform (FFT) instead. It is well known that DFT transforms a time-domain sequence into a frequency-domain representation as illustrated by Figure 13. The DFT of a discrete-time signal $x[n]$ is defined as

$$X_k = \sum_{n=0}^{N-1} x\,[n] e^{-j(2\pi/N)nk}, k = 0, 1, \ldots, N-1,$$

where N is the sample size and $j = \sqrt{-1}$. Similar to all the aforementioned extracted signal features, the DFT peak amplitude features are quite sensitive to any scaling factor and hence they have to be normalized by the respective feature obtained from the zero-stress specimen [13].

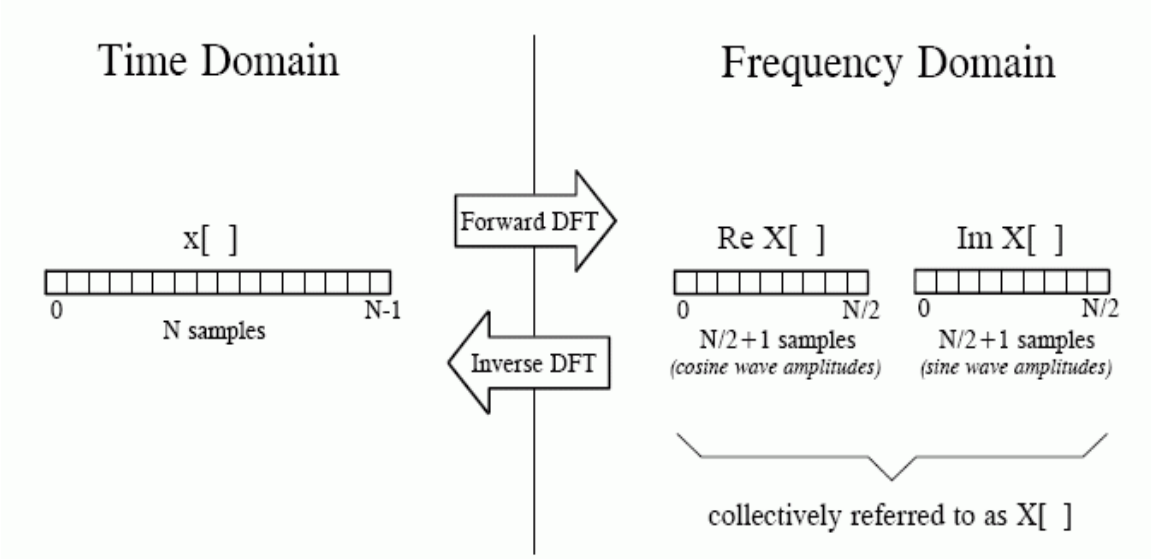

Figure 13. Illustration of the frequency analysis using DFT (duplicated from [14] with the permission from the authors).

3.2.2.3 Chirp-Z Transform (CZT)

CZT is a frequency transform similar to DFT and is a generic case for the *Z*-transform [15]. It is also called *Bluestein's FFT Algorithm*. CZT is an algorithm that evaluates the *Z*-transform of a signal sequence [16]. CZT establishes the *Z*-transform along the spiral contours in the *z*-plane for an arbitrary signal sequence $x[n]$ [17]. The *Z*-transform of a sequence $x[n]$ is defined as

$$X(z) = \sum_{n=-\infty}^{\infty} x[n]z^{-n}$$

The *Z*-transform is usually sampled along the unit circle (|*z*|=1) and it will be reduced to the discrete-time Fourier transform (DTFT). The DTFT has a lot of applications for spectral estimation, filtering, interpolation, and correlation [16]. The *Z*-transform of a finite-support sequences is defined as

$$X(z) = \sum_{n=0}^{N-1} x[n]z^{-n},$$

where *N* is the sequence length. Thus, one may sample the *Z*-transform on a finite set of points z_k as given by

$$X(z_k) = \sum_{n=0}^{N-1} x[n]z_k^{-n}$$

Obviously, DFT is a special case where the set of points are equally spaced along the unit circle such that

$$z_k = exp\ (j2\pi k/N),\ k = 0,\ 1,\ldots\ldots,\ N\text{-}1.$$

In a similar manner, the CZT can be defined by sampling the *Z*-transform along a general contour where $z_k = AW^{-k}$, k = 0, 1,.., M-1 and M is an arbitrary positive integer. The parameters A and W are two arbitrary complex numbers such that

$$A = A_0 e^{j2\pi\theta_0},$$

$$W = W_0\, e^{j2\pi\varphi_0},$$

where θ_0 and φ_0 are the *initial angular frequency* and *angular frequency increment* values, respectively.

Thus, the CZT of a sequence $x[n]$ is given by

$$CZT(x[n]) = \sum_{n=0}^{N-1} x[n]\ z_k{}^{-n}$$

The corresponding peak amplitudes are considered as features for yield detection in this thesis work. Similarly, the chirp-*Z*-transform features are quite sensitive to any scaling factor and hence they have to be normalized by the respective features obtained from the zero-stress specimen [13].

3.2.2.4 Discrete Cosine Transform (DCT)

Discrete cosine transform (DCT) [17] is equivalent to the DFT of a periodically extended sequence from the original signal, which possesses the even symmetry. It belongs to the family of sinusoidal unitary transforms, which are real, orthogonal, and separable with fast computation algorithms [18]. The commonly used variant of DCT is the Type-II DCT which we often just call as "DCT" [20]. The DCT of a discrete-time signal $x[n]$ is defined as

$$y(k) = w(k) \sum_{n=1}^{N} x(n) \cos\left(\frac{\pi (2n-1)(k-1)}{2N}\right), \; k = 1, 2 \ldots N,$$

where $w(k) = \frac{1}{\sqrt{N}}$ for $k = 1$ and $w(k) = \sqrt{\frac{2}{N}}$ for $2 \leq k \leq N$.

The DCT has applications in signal and image processing because of its property of concentrating the energy of the signal in the low DCT bins [20]. According to [21], DCT is also used for data compression. The dominant DCT coefficients for signal echoes are considered as the features for the yield analysis. Similar to other signal features, the DCT features are quite sensitive to any scaling factor and hence they have to be normalized by the respective DCT features obtained from the zero-stress specimen [13].

3.2.2.5 Discrete Sine Transform (DST)

Discrete sine transform (DST) is equivalent to the DFT of a periodically extended sequence from the original signal, which possesses the odd symmetry. The DST also belongs to

the family of unitary sinusoidal transforms [22] and it has orthogonal sine basis functions. The commonly used variant of the DST is the Type–I DST which we usually simply call as "DST". The DST of a discrete-time signal $x[n]$ is defined as

$$y(k) = \sum_{n=1}^{N} x[n] \sin\left(\frac{\pi kn}{N+1}\right), \; k = 1, 2\ldots, N,$$

where N is the length of $x[n]$.

Some of the DST variants are used in applications of the fast implementation of lapped orthogonal transform for efficient transform/subband coding [24]. The dominant DST coefficients for signal echoes are used as the features for the yield analysis. Similarly, the DST features are quite sensitive to any scaling factor and hence they have to be normalized by the respective DST features obtained from the zero-stress specimen [13].

3.3 Linear Discriminant Analysis

In this thesis, we propose to adopt the *linear discriminant analysis* (*LDA*) technique to extract the "optimal" features for yield detection. LDA is a classical multivariate statistical technique used in pattern classification and analysis. LDA facilitates a linear combination of features in the lower-dimensional subspace and helps classify two or more classes more accurately in this subspace [25]. Two important measures are evaluated using all data samples, namely the *within class scatter matrix* and the *between class scatter matrix*.

The objective of the LDA technique is to maximize the *between class measure* while minimizing the *within class measure*. According to [26], the criterion function that has to be maximized is called the *"Fisher's Criterion"*, which is given by

$$J(w) = argmax \; v_k S_B v_k^T \text{ s. t. } v_k S_w v_k^T = 1,$$

where S_B is the between class scatter matrix and S_W is the within class scatter matrix as given by

$$S_B = \sum_{i=1}^{c} |\chi_i| (\mu_i - \mu)\ (\mu_i - \ \mu)^T,$$

$$S_W = \sum_{i=1}^{c} \sum_{x_k \in \chi_i} (x_k - \mu_i)(\mu_k - \mu_i)^T,$$

c is the number of classes, μ_i is the mean of the class χ_i, and $|\chi_i|$ is the number of samples of class χ_i. Thus LDA is to find the projection in the lower-dimensional subspace where the Fisher's Criterion related to the between class scatter matrix and the within class scatter matrix is maximized. The corresponding solution is equivalent to the solution to the *generalized eigen-decomposition* problem as follows:

$$S_B v_k = \lambda_k S_W v_k, \text{ for } k = 1, 2, \ldots, m,$$

where λ_k and v_k are the k^{th} respective eigenvalue and eigenvector.

In the literature, LDA technique is used as a popular pattern recognition technique for defect detection. In [27], LDA was proposed as a pattern recognition technique to extract defect features for the magnetic flux leakage NDT. Also in [28], LDA was used to classify the AISI 420 steel samples subjected to different heat treatments using magnetic Barkhausen noise signals. Actually, most research on NDT for SHM using LDA is focused on defect detection and material property characterization.

In this study of yield detection, LDA is adopted to integrate the obtained signal features from the two classes (No-Yield data and Yield data) and its performance is evaluated. The data set used for this study consists of 183 individual ultrasonic signal waveforms and three dominant echoes are spotted for each signal waveform; from each echo, we can extract nine different kinds of features. Hence we have a total number of 183 signals × 3 echoes/signal × 9 features/echo = 549 features. The feature vector extracted from each ultrasonic signal echo is thus given by

$$\begin{bmatrix} Signal\ Peak\ Amplitude \\ Signal\ Energy \\ Wavelet\ Peak\ Amplitude \\ Wavelet\ Peak\ to\ Peak\ Amplitude \\ Wavelet\ RMS\ Amplitude \\ FFT\ Peak\ Amplitude \\ CZT\ Peak\ Amplitude \\ DCT \\ DST \end{bmatrix}$$

Note that among 183 original ultrasonic signal waveforms, 89 of them belong to the "No-Yield" class and 94 of them belong to the "Yield" class. Therefore, 267 feature vectors are extracted to represent the "No-Yield" condition while the other 282 feature vectors are extracted to represent the "Yield" condition. We randomly pick 242 feature vectors subject to the "No-Yield" condition and 257 feature vectors subject to the "Yield" condition for training and leave 25 feature vectors subject to the "No-Yield" condition and 25 feature vectors subject to the "Yield" condition for testing.

Then we employ the LDA projector onto the training feature vectors to seek the one-dimensional subspace (m=1) for maximizing the Fisher's Criterion. Figure 14 depicts the projections of the two classes onto this optimal subspace. From Figure 14, it can be inferred that there exhibits a quite good distinction between these two classes with the help of LDA. Hence a simple threshold can be used to well separate the two classes in this subspace. In this example, the threshold can be set to a value between -0.1 and 0 leading to a good separation of the two classes.

We also project the testing feature vectors onto the same subspace. Figure 15 demonstrates those projections resulting from the training data in the two classes as well as the projections resulting from the test data onto the LDA subspace. The threshold established using

the training feature vectors is used to classify any test data into either of the "No-Yield" and "Yield" classes. We will provide more detailed analysis on the experimental results in next chapter.

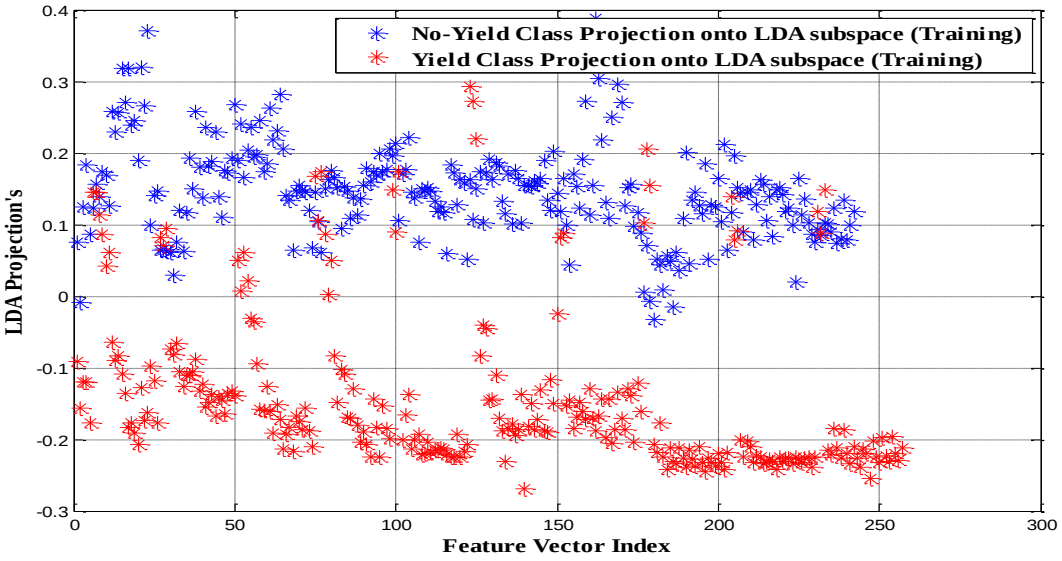

Figure 14. Illustration of LDA projections for training feature vectors.

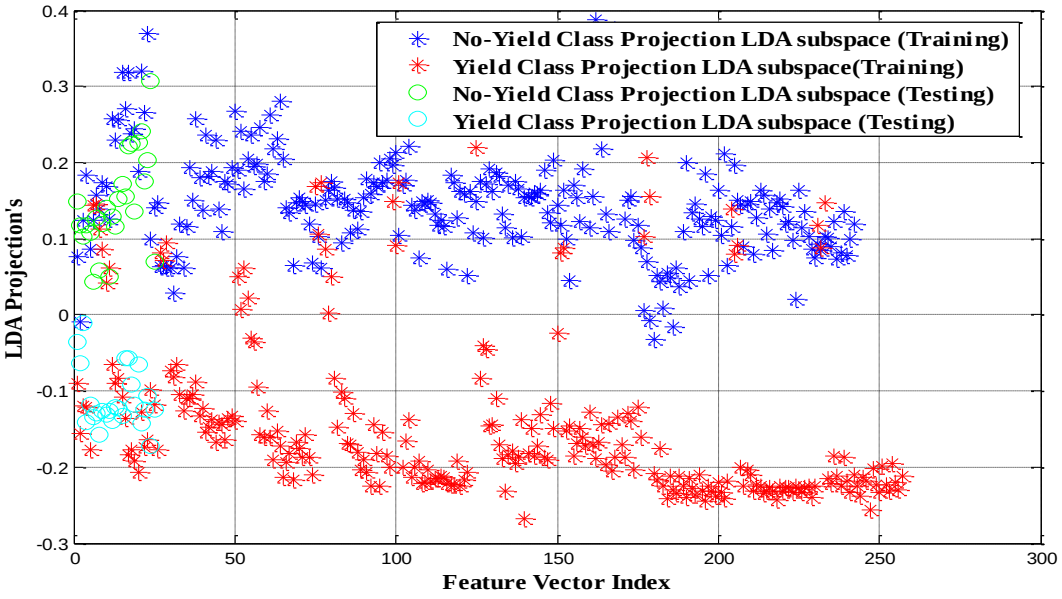

Figure 15. Illustration of LDA projections for both training and testing feature vectors.

CHAPTER 4: COMPARITIVE STUDY ON THE EXTRACTED SIGNAL FEATURES AND LINEAR DISCRIMINANT ANALYSIS FOR YIELD DETECTION

This chapter discusses the experimental results obtained from the extracted signal features for yield detection. Based on experimental results, graphical and statistical analyses of the extracted signal features are investigated. Scatter plots are delineated for graphical analysis and the two main statistical descriptors, namely mean and standard deviation, are evaluated for the extracted signal features. This chapter also presents the ROC plots regarding every kind of features and the proposed LDA technique for yield detection.

4.1 Experimental Results for Signal Features

The experimental results are first visualized using the graphical analysis. For the graphical analysis, the scatter plots are demonstrated for the aforementioned signal features. In a scatter plot, the horizontal axis represents the percentage of stress applied while the vertical axis indicates the signal feature value for yield detection. The percentage of stress applied on the testing specimen is divided into three stress intervals. In the scatter plots, they are: (*i*) 0-100% of stress applied – *red circles*, (*ii*) 100-115% of stress applied – *blue triangles*, and (*iii*) more than 115% of stress applied – *yellow squares*.

4.2 Graphical Analysis of Time-Domain Signal Features

4.2.1 Peak Amplitude

Figure 16 shows the scatter plot for the first time-domain signal feature, i.e., peak amplitude. From Figure 16, it can be discovered that the peak amplitude changes as the stress level varies. The peak amplitude stays within the range of [0.5, 1.6] when 0-100% of stress is applied. When the applied stress gets larger, the peak amplitude has an obvious drop till the

stress level reaches 105%. When more than 105% of stress is applied, the peak amplitude stays within [0.1, 0.6].

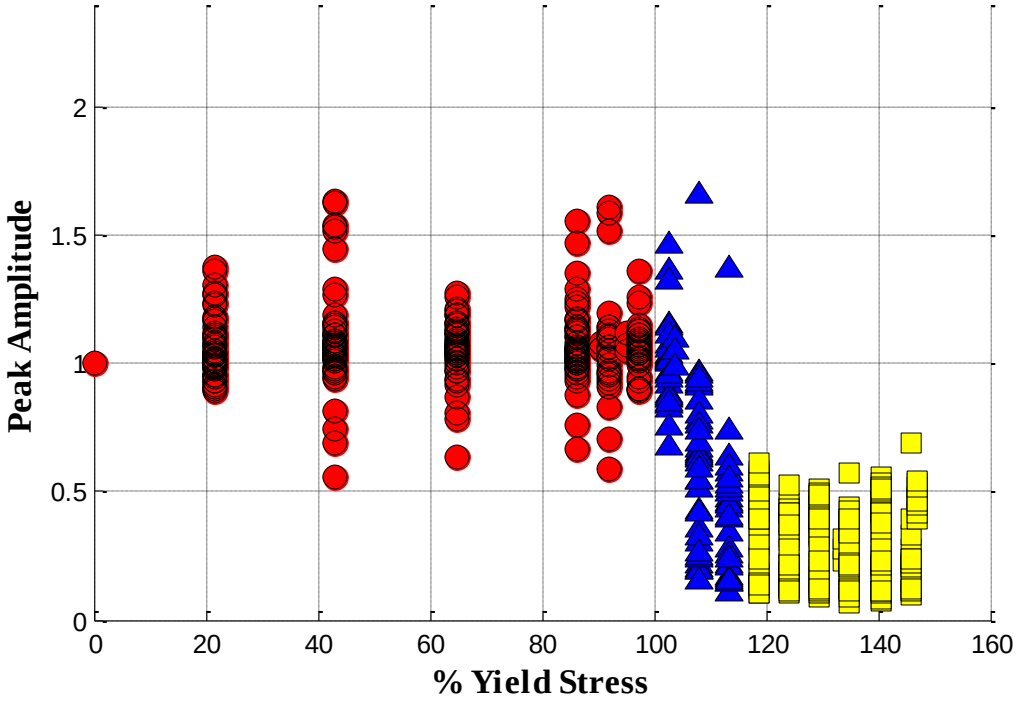

Figure 16. Scatter plot for peak amplitude.

4.2.2 Signal Energy

Figure 17 shows the scatter plot for the second time-domain signal feature, i.e., signal energy. From Figure 17, it can be inferred that the signal energy changes as the stress level varies. In the stress range of 0-100%, the signal energy values fall within the range of [0.4, 2.2]. When the stress level keeps going up within the range of 100-115%, the corresponding signal energy very often declines. As the stress levels reach beyond 105%, the signal energy values settle within the range of [0, 1.6]. Then the signal energy keeps reducing when the stress level is larger than 115%. According to [13], it is due to the fact that errors often arise in the measurement for the unstressed specimen.

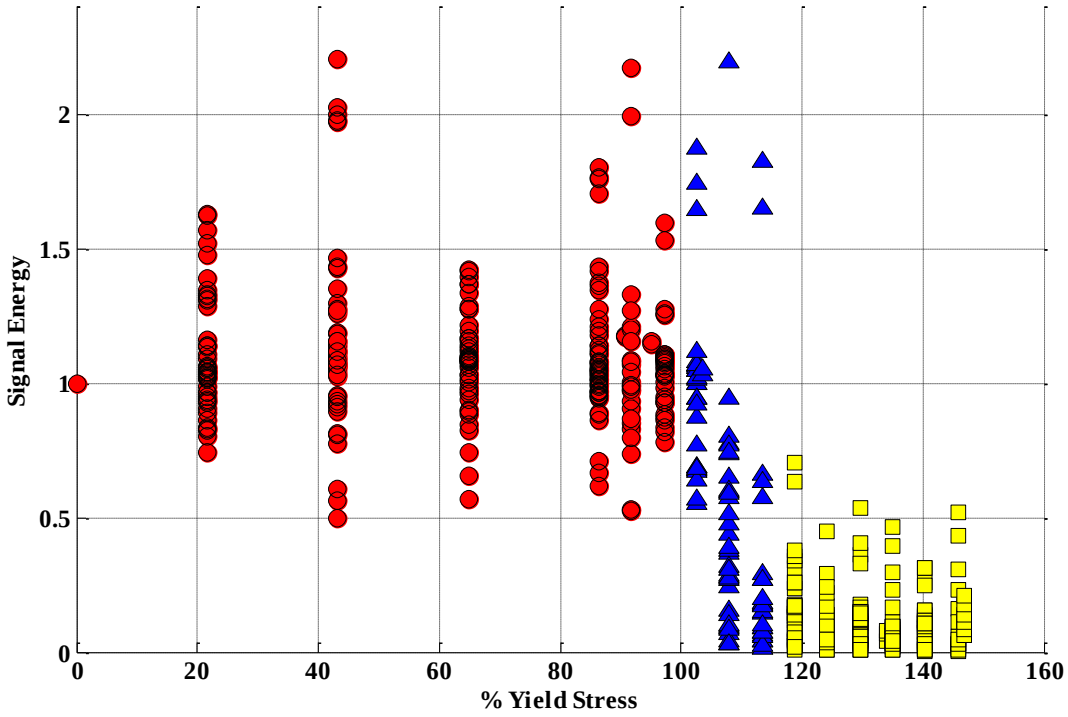

Figure 17. Scatter plot for signal energy.

4.3 Graphical Analysis of Transform-Domain Signal Features

4.3.1 Wavelet Features (Wavelet Peak Amplitude, Wavelet Peak-to-Peak Amplitude, Wavelet RMS Amplitude)

Figures 18, 19, and 20 exhibit the scatter plots for the wavelet features subject to the wavelet "bi-orthogonal 1.3". Figure 18 shows the scatter plot for the wavelet peak amplitude. According to Figure 18, it can be discovered that the wavelet peak amplitudes fall within the range [0.5, 1.6] when the stress intervals 0-105% are applied. The wavelet peak amplitudes decrease as the stress levels go beyond 105%. The wavelet peak amplitudes lie within the range of [0.1, 1.5] when the stress levels are 105-115%. The wavelet peak amplitudes then drop in the range of [0.1, 0.6] as the applied stress levels reach higher than 115%.

Figure 19 shows the scatter plot for the wavelet peak-to-peak amplitude. From Figure 19, it can be discovered that the wavelet peak-to-peak amplitudes lie within the range of [0.6, 1.6]

when 0-105% of the stress intervals are applied. As the stress levels increase beyond 105%, the wavelet peak-to-peak amplitudes fall within [0.1, 1.6]. When the stress levels go above 115%, the wavelet peak-to-peak amplitudes tend to decrease and the values are in range of [0.1, 0.5].

Figure 20 depicts the scatter plot for the wavelet RMS amplitude. When 0-100% of the stress levels are applied, the wavelet RMS amplitudes lie within the range of [0.6, 1.8]. When the stress levels are 100-115%, the wavelet RMS amplitudes slightly reduce and lie in range of [0.2, 1.6]. As the stress levels reach above 115%, the wavelet RMS amplitudes decrease more and fall within the range of [0.1, 0.9].

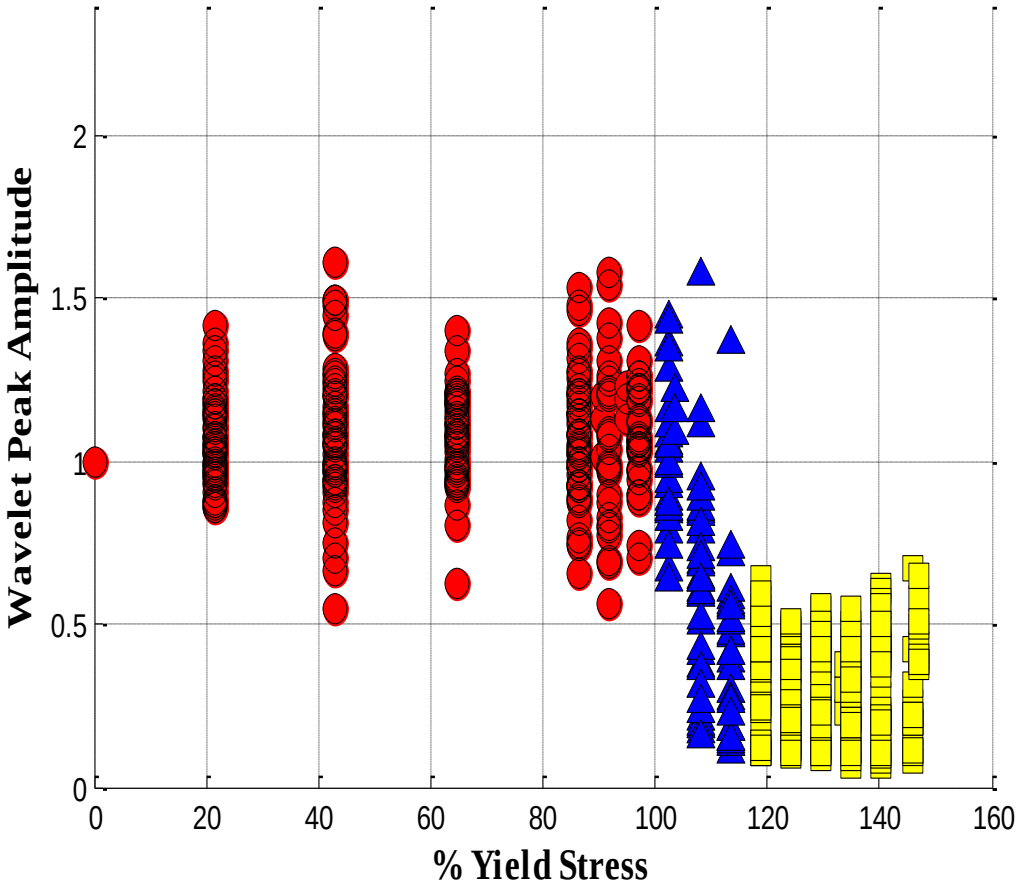

Figure 18. Scatter plot for wavelet peak amplitude.

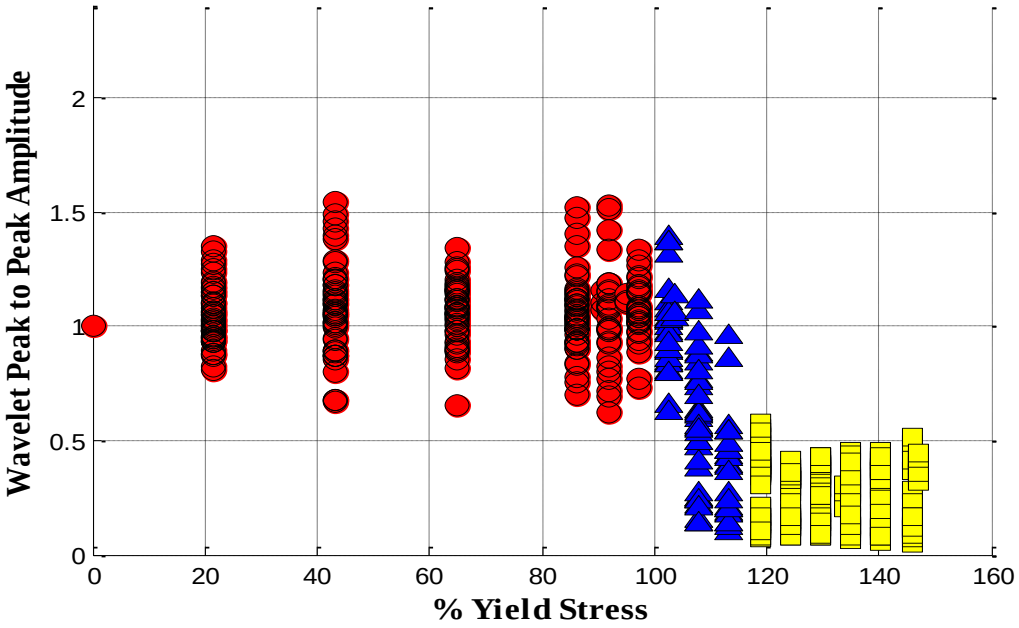

Figure 19. Scatter plot for wavelet peak-to-peak amplitude.

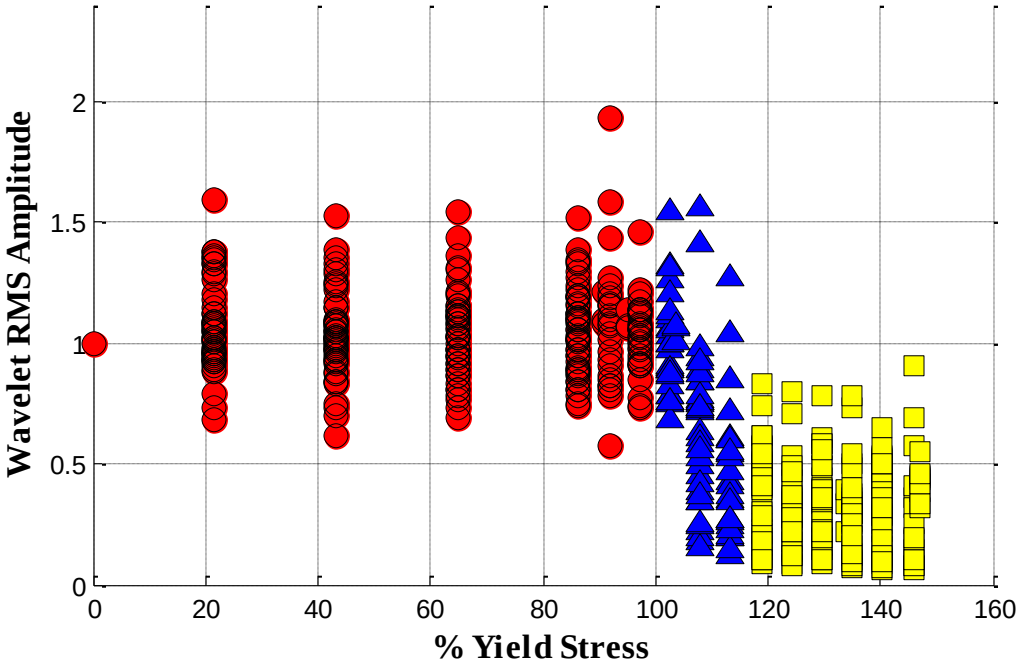

Figure 20. Scatter plot for wavelet RMS amplitude.

4.3.2 FFT Peak Amplitude

Figure 21 shows the scatter plot for the FFT peak amplitude. From Figure 21, it can be discovered that the FFT peak amplitudes lie within the range of [0.45, 2.2] when the stress levels are 0-100%. When the stress levels reach up to 100-115%, the FFT peak amplitudes drop and lie in the range of [0.2, 1.6]. As more stresses (larger than 115%) are applied, the FFT peak amplitudes further decrease and fall within the range of [0.1, 1.4].

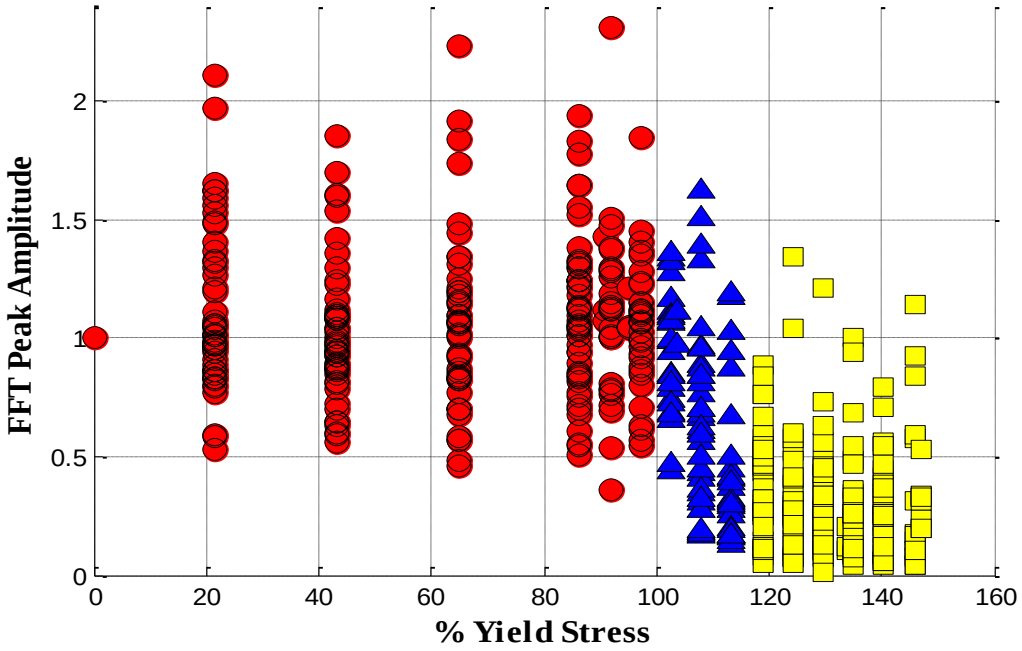

Figure 21. Scatter plot for FFT peak amplitude.

4.3.3 CZT Peak Amplitude

We depict the scatter plot for CZT peak amplitude in Figure 22. From Figure 22, it can be discovered that the CZT peak amplitudes lie within the range of [0.6, 1.8] when the stress levels are 0-100%. When the stress levels increase up to 100-115%, the CZT peak amplitudes drop and fall in the range of [0.2, 2.2]. As more stresses (higher than 115%) are applied, the CZT peak amplitudes further decrease and lie within the range of [0.1, 1.3].

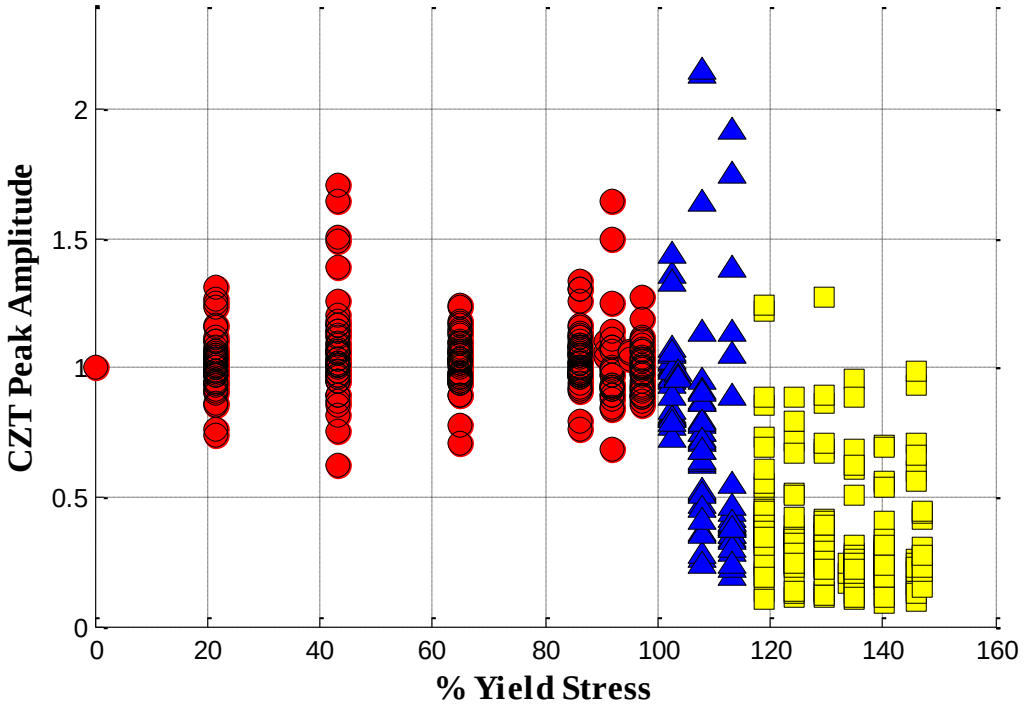

Figure 22. Scatter plot for CZT peak amplitude.

4.3.4 Dominant DCT Coefficient

Figure 23 shows the scatter plot for the DCT coefficients employed for the yield analysis. It can be observed from Figure 23 that the dominant DCT coefficients lie in the range of [0.5, 2.1] when the stress levels are within 0-100%. When the stress levels reach up to 100-115%, the dominant DCT coefficients drop and fall within the range of [0.2, 2.1]. The dominant DCT coefficients further decrease and lie in the range of [0.1, 1.4] for the stress levels above 115%.

4.3.5 Dominant DST Coefficient

Figure 24 exhibits the scatter plot for the DST coefficients. According to Figure 24, it can be discovered that when the stress levels are applied within 0-100%, the dominant DST coefficients lie in the range of [0.4, 1.6]. As the stress levels go up to 100-115%, the dominant

DST coefficients drop and fall within the range of [0.2, 2.2]. As the stress levels increase above 115%, the dominant DST coefficients further decrease and lie in the range of [0.1, 0.9].

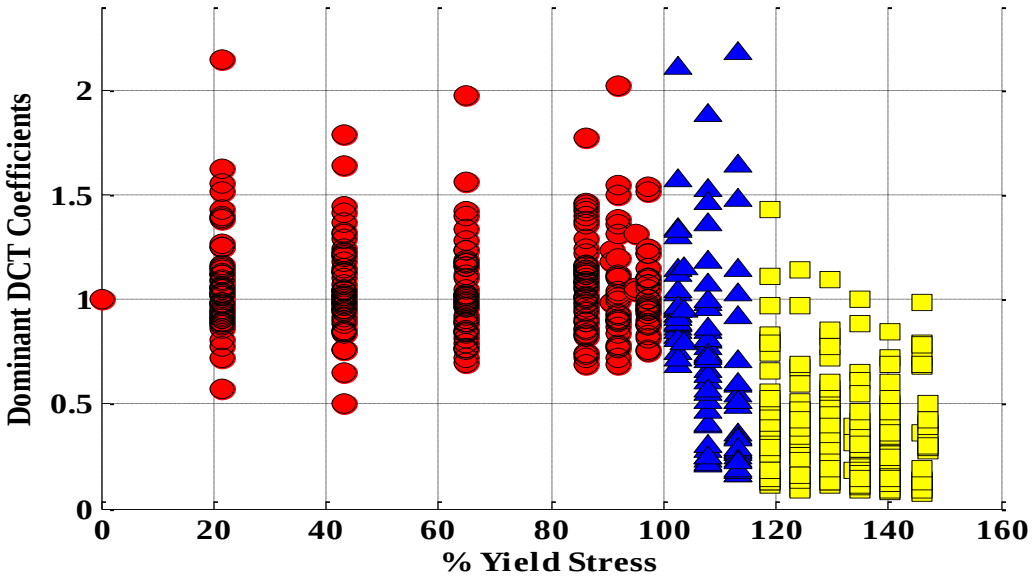

Figure 23. Scatter plot for dominant DCT coefficient.

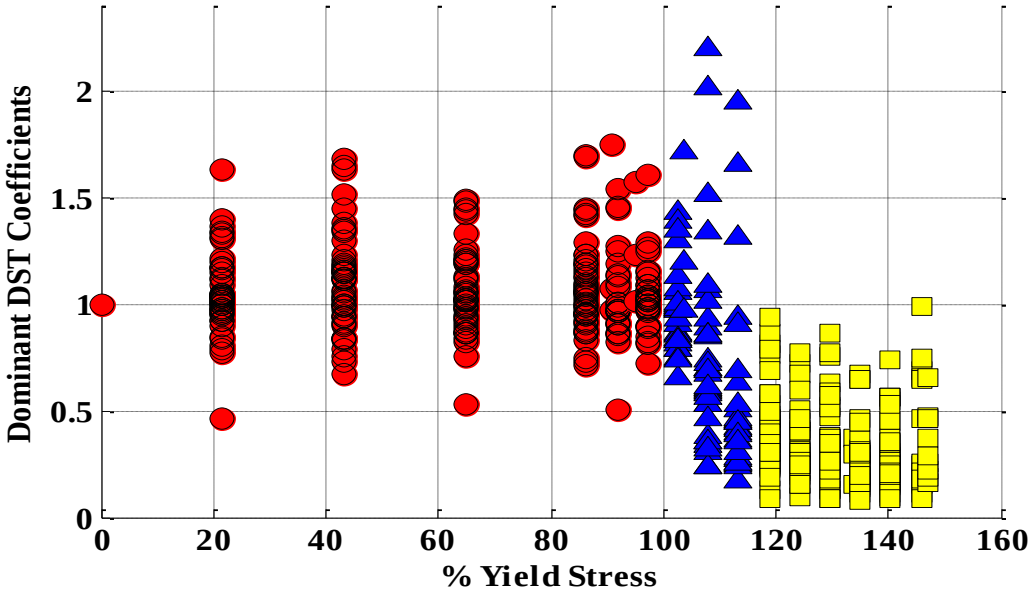

Figure 24. Scatter plot for dominant DST coefficient.

4.4 Statistical Analysis (Mean and Standard Deviation) of the Signal Features

Apart from the graphical analysis of the signal features for various stress levels, the basic statistical analysis is also carried out here. Two statistical measures investigated for the signal features are *mean* and *standard deviation*. Table 2 lists the mean and standard deviation (briefed as "SD") values for the signal features calculated from the ultrasound echoes.

Table 2. Statistical Measures for Signal Features

Features	Statistical Measures	*0-100% Yield Stress*	*100-115% Yield Stress*	*Above 115% Stress*
Peak Amplitude	Mean	1.0681	0.6732	0.3141
	SD	0.1545	0.3553	0.1447
Signal Energy	Mean	1.1160	0.5960	0.1225
	SD	0.2883	0.5209	0.1209
Wavelet Peak Amplitude	Mean	1.0771	0.6805	0.3188
	SD	0.1833	0.3656	0.1550
Wavelet Peak-to-Peak Amplitude	Mean	1.0598	0.6420	0.2749
	SD	0.1627	0.3459	0.1303
Wavelet RMS Amplitude	Mean	1.0527	0.6963	0.3401
	SD	0.1863	0.3523	0.1792
FFT Peak Amplitude	Mean	1.0731	0.7249	0.3246
	SD	0.3267	0.4531	0.2408
CZT Peak Amplitude	Mean	1.0350	0.7717	0.3630
	SD	0.1387	0.4071	0.2286
Dominant DCT Coefficient	Mean	1.0645	0.7955	0.3823
	SD	0.2357	0.4754	0.2485
Dominant DST Coefficient	Mean	1.0664	0.7741	0.3508
	SD	0.2076	0.4220	0.1920

4.5 Performance Analysis of Signal Features -Receiver Operating Characteristics (ROC)

The graphical analysis presented in Section 4.3 shows the good separability between the no-yield and yield classes using any of the aforementioned signal features. On the other hand, the performances of the aforementioned signal features used for yield detection should be evaluated using the *receiver operating characteristics* (ROC) curves. An ROC curve is a plot of the true positive rate versus the false positive rate. The true positive rate (probability of correct detection) and the false positive rate (probability of false detection or false alarm) are defined as

$$\textit{True Positive Rate } (TPR) = \frac{Number\ of\ correctly\ classified\ positives}{Number\ of\ positives},$$

$$\textit{False Positive Rate } (FPR) = \frac{Number\ of\ incorrectly\ classified\ negatives}{Number\ of\ negatives},$$

respectively.

In this thesis, the ROC curves are all plotted for using the extracted signal features to distinguish between the yield and no-yield conditions. We take two cases to differentiate these two conditions. They are

Case1: No-Yield: 0-100% of stress is applied; Yield: above 100% of stress is applied. The corresponding ROC curve is colored blue.

Case2: No-Yield: 0-115% of stress is applied; Yield: above 115% of stress is applied. The corresponding ROC curve is colored red.

In the following subsections, all the extracted signal features for the yield analysis are evaluated. Tables 3 and 4 list the true positive rates and the corresponding false positive rates for peak amplitude and signal energy, respectively. Figures 25 and 26 delineate the respective ROC curves. Tables 5-11 list the true positive rates and the corresponding false positive rates for wavelet peak amplitude, wavelet peak-to-peak amplitude, wavelet RMS amplitude, FFT peak

amplitude, CZT peak amplitude, dominant DCT coefficient, and dominant DST coefficient, respectively. Figures 27-33 exhibit the corresponding ROC curves for these seven features.

4.5.1 ROC Analysis – Peak Amplitude

Table 3. ROC Table for Peak Amplitude

ROC Analysis: Case1

Threshold	TPR (%)	FPR (%)
0.0	0	0
0.2	21.2	0
0.4	53.19	0
0.6	80.8	0.7
0.8	86.87	3.37
1.0	93.26	25.09
1.2	98.22	88.01
1.4	99.29	95.88
1.6	99.64	99.88
1.8	100	100
2.0	100	100
2.2	100	100
2.4	100	100

ROC Analysis: Case 2

Threshold	TPR (%)	FPR (%)
0.0	0	0
0.2	26.98	2.5
0.4	66.6	6.6
0.6	98.94	11.94
0.8	100	18.05
1.0	100	39.16
1.2	100	89.72
1.4	100	96.38
1.6	100	98.88
1.8	100	100
2.0	100	100
2.2	100	100
2.4	100	100

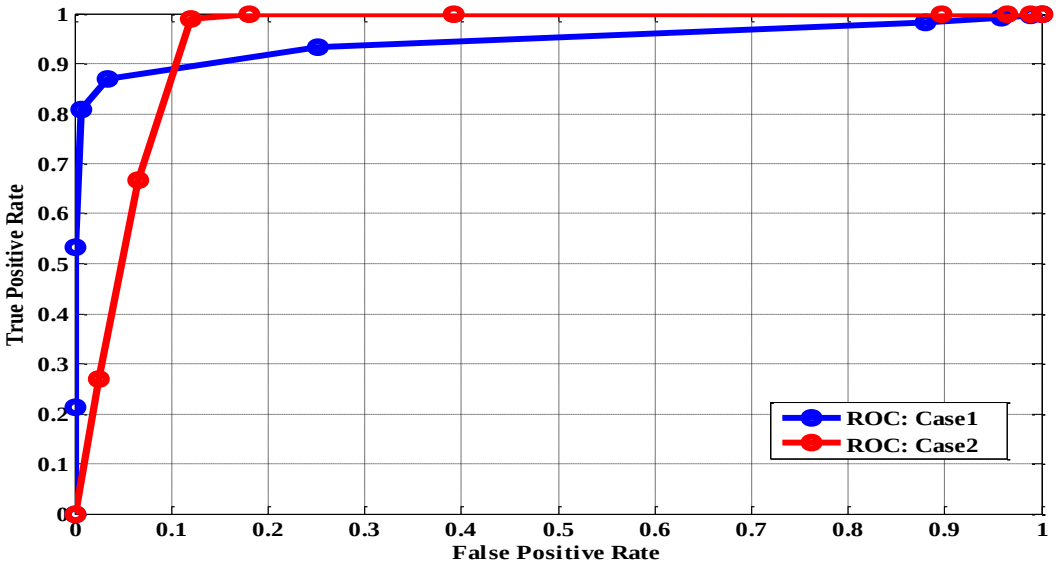

Figure 25. ROC curves for peak amplitude.

4.5.2 ROC Analysis – Signal Energy

Table 4. ROC Table for Signal Energy

ROC Analysis: Case1

Threshold	TPR (%)	FPR (%)
0.0	0	0
0.2	66.31	0
0.4	79.07	0
0.6	84.4	1.87
0.8	90.42	5.99
1.0	93.26	31.08
1.2	97.5	76.02
1.4	97.5	89.13
1.6	97.5	94.38
1.8	98.58	96.25
2.0	99.29	97.75
2.2	99.64	98.87
2.4	99.64	99.25
2.6	100	100

ROC Analysis: Case 2

Threshold	TPR (%)	FPR (%)
0.0	0	0
0.2	83.59	8.05
0.4	95.76	11.66
0.6	98.94	15.55
0.8	100	22.77
1.0	100	43.61
1.2	100	80.27
1.4	100	90
1.6	100	93.88
1.8	100	96.11
2.0	100	97.77
2.2	100	98.88
2.4	100	99.16
2.6	100	100

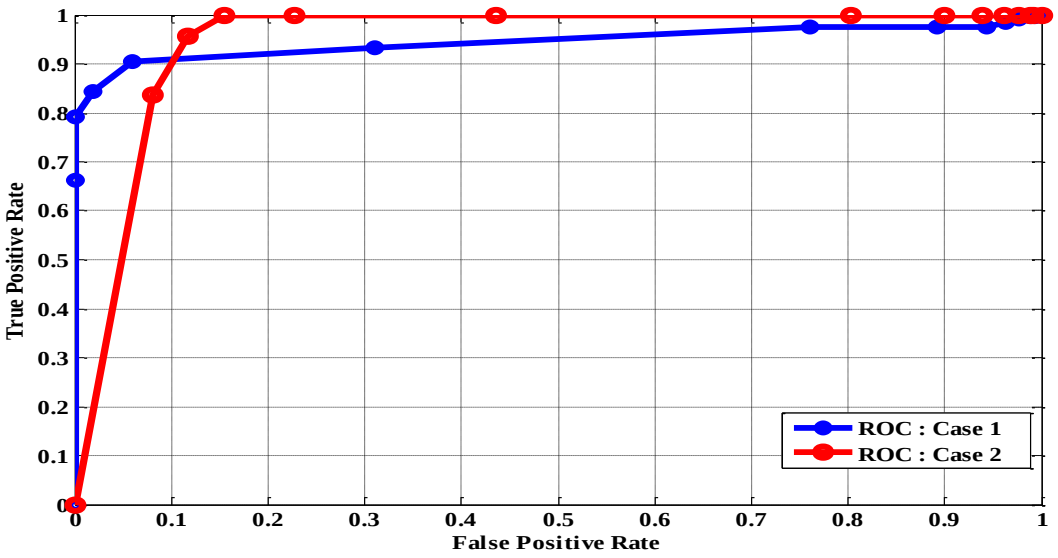

Figure 26. ROC curves for signal energy.

4.5.3 ROC Analysis – Wavelet Peak Amplitude

Table 5. ROC Table for Wavelet Peak Amplitude

ROC Analysis: Case1

Threshold	TPR (%)	FPR (%)
0.0	0	0
0.2	21.98	0
0.4	51.4	0
0.6	79.07	0.74
0.8	86.87	5.99
1.0	93.26	34.83
1.2	97.16	75.28
1.4	98.94	94.75
1.6	100	99.62
1.8	100	100
2.0	100	100
2.2	100	100
2.4	100	100

ROC Analysis: Case2

Threshold	TPR (%)	FPR (%)
0.0	0	0
0.2	26.98	3.05
0.4	64.02	6.6
0.6	96.82	11.66
0.8	100	20
1.0	100	46.38
1.2	100	79.44
1.4	100	95.27
1.6	100	99.72
1.8	100	100
2.0	100	100
2.2	100	100
2.4	100	100

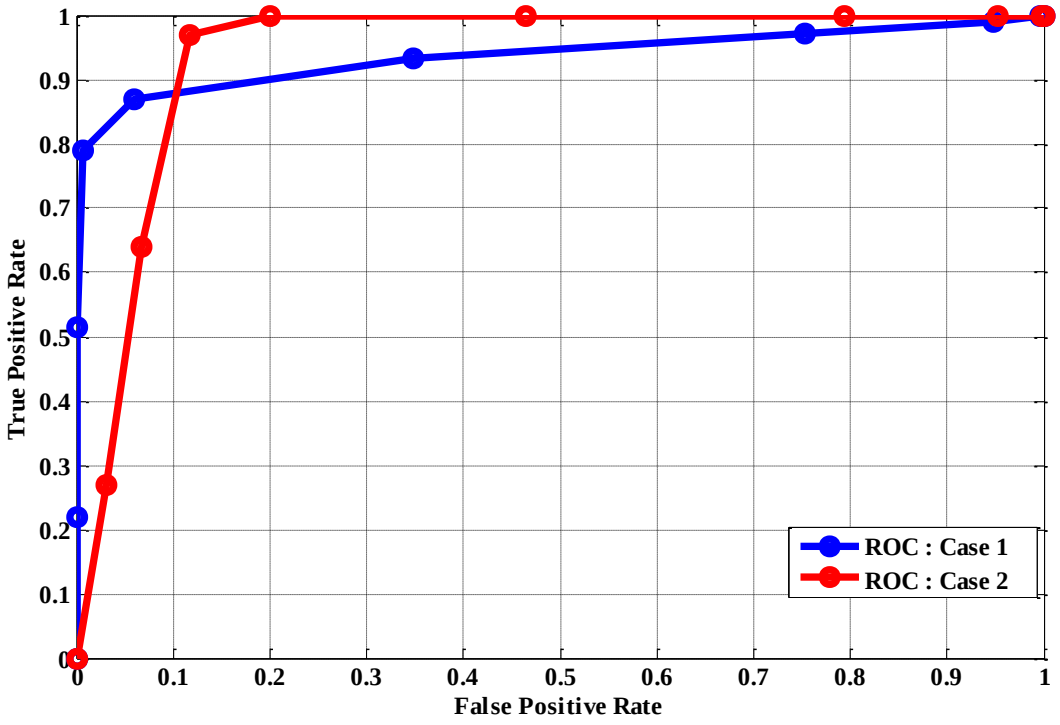

Figure 27. ROC curves for wavelet peak amplitude.

4.5.4 ROC Analysis – Wavelet Peak-to-Peak Amplitude

Table 6. ROC Table for Wavelet Peak-to-Peak Amplitude

ROC Analysis: Case1

Threshold	TPR (%)	FPR (%)
0.0	0	0
0.2	28.3	0
0.4	64.18	0
0.6	82.9	0
0.8	87.23	5.24
1.0	93.97	33.3
1.2	98.58	85.01
1.4	100	96.2
1.6	100	100
1.8	100	100
2.0	100	100
2.2	100	100
2.4	100	100

ROC Analysis: Case 2

Threshold	TPR (%)	FPR (%)
0.0	0	0
0.2	36	3.3
0.4	82.01	7.22
0.6	100	12.5
0.8	100	19.72
1.0	100	45.8
1.2	100	87.7
1.4	100	97.22
1.6	100	100
1.8	100	100
2.0	100	100
2.2	100	100
2.4	100	100

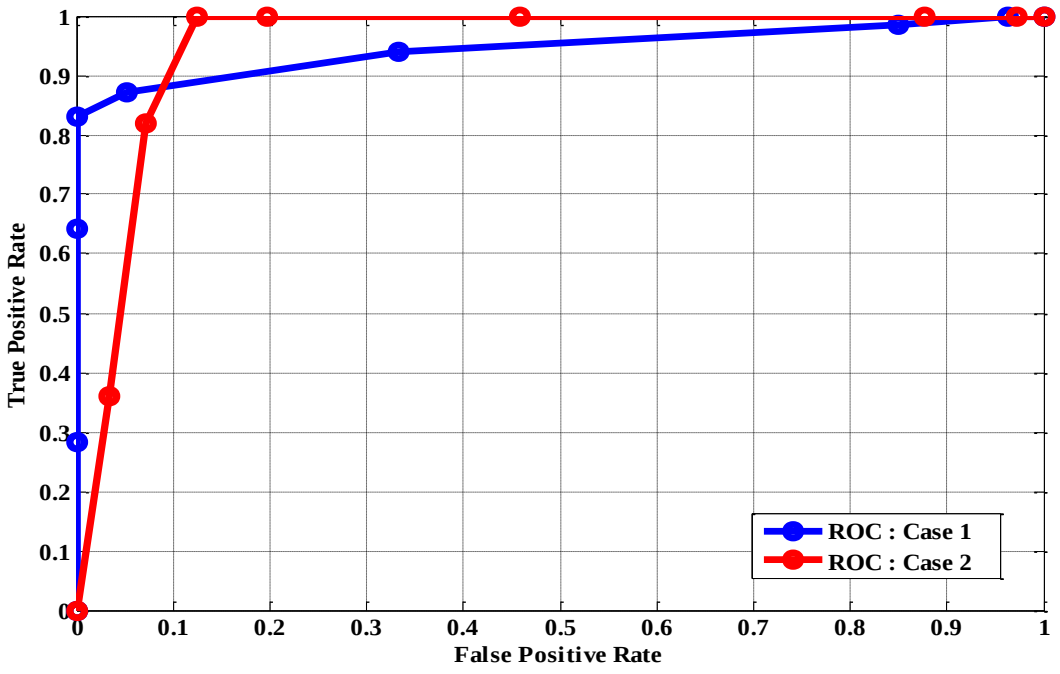

Figure 28. ROC curves for wavelet peak-to-peak amplitude.

4.5.5 ROC Analysis – Wavelet RMS Amplitude

Table 7. ROC Table for Wavelet RMS Amplitude

ROC Analysis: Case1

Threshold	TPR (%)	FPR (%)
0.0	0	0
0.2	20.2	0
0.4	51.77	0
0.6	75.53	0.3
0.8	86.52	7.1
1.0	93.61	37.82
1.2	97.16	81.64
1.4	98.93	96.62
1.6	100	99.62
1.8	100	99.62
2.0	100	100
2.2	100	100
2.4	100	100

ROC Analysis: Case2

Threshold	TPR (%)	FPR (%)
0.0	0	0
0.2	25.9	2.2
0.4	64.55	6.66
0.6	93.12	10.55
0.8	98.9	21.11
1.0	100	48.88
1.2	100	84.16
1.4	100	96.66
1.6	100	99.72
1.8	100	99.72
2.0	100	100
2.2	100	100
2.4	100	100

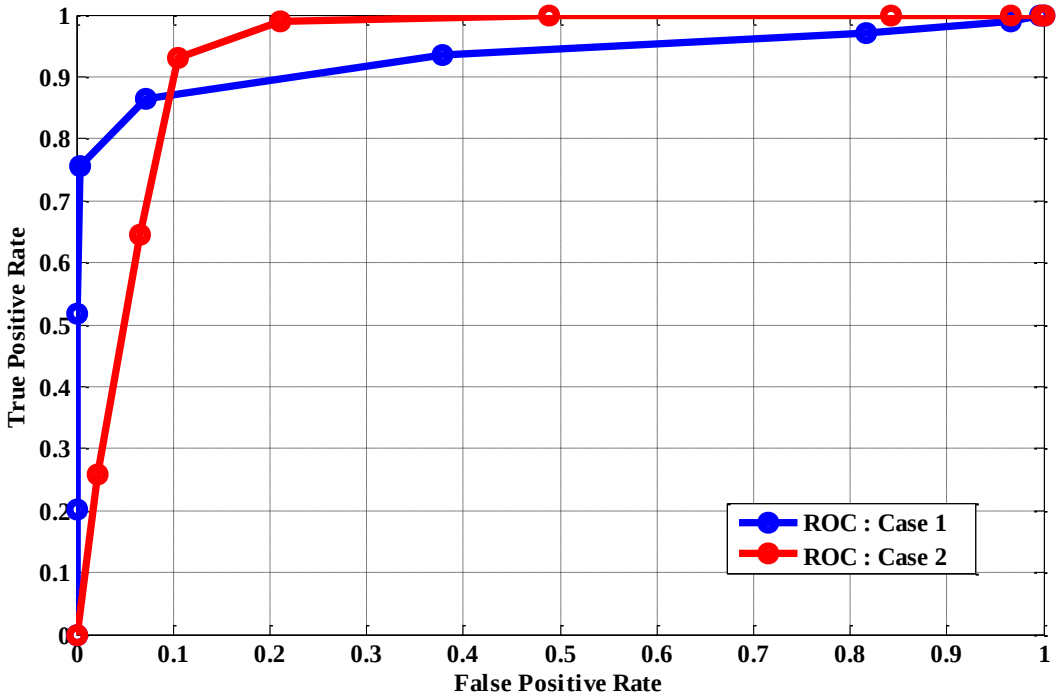

Figure 29. ROC curves for wavelet RMS amplitude.

4.5.6 ROC Analysis – FFT Peak Amplitude

Table 8. ROC Table for FFT Peak Amplitude

ROC Analysis: Case1

Threshold	TPR (%)	FPR (%)
0.0	0	0
0.2	27	0
0.4	57.1	0.3
0.6	74.4	6.3
0.8	82.26	17.9
1.0	95.7	42.3
1.2	98.6	71.5
1.4	98.9	86.14
1.6	99.2	92.88
1.8	99.2	96.25
2.0	99.2	98.87
2.2	99.2	99.25
2.4	99.2	100
2.6	100	100

ROC Analysis: Case2

Threshold	TPR (%)	FPR (%)
0.0	0	0
0.2	33.86	3.3
0.4	70.89	7.7
0.6	90.47	15.55
0.8	94.7	28.05
1.0	97.35	51.1
1.2	98.94	76.11
1.4	100	88.61
1.6	100	93.88
1.8	100	96.66
2.0	100	98.61
2.2	100	98.88
2.4	100	99.44
2.6	100	100

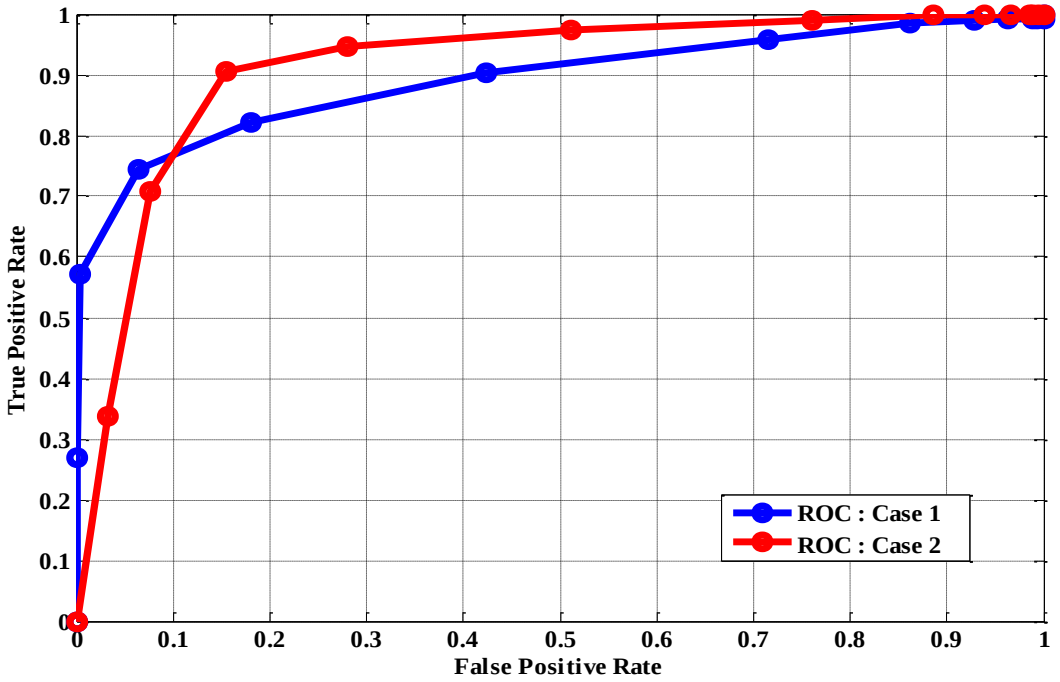

Figure 30. ROC curves for FFT peak amplitude.

4.5.7 ROC Analysis – CZT Peak Amplitude

Table 9. ROC Table for CZT Peak Amplitude

ROC Analysis: Case1

Threshold	TPR (%)	FPR (%)
0.0	0	0
0.2	12.41	0
0.4	56.73	0
0.6	68.79	0
0.8	80.85	3.3
1.0	92.19	39.3
1.2	95.7	91.7
1.4	97.8	97.7
1.6	98.22	98.87
1.8	98.9	100
2.0	99.2	100
2.2	100	100
2.4	100	100

ROC Analysis: Case2

Threshold	TPR (%)	FPR (%)
0.0	0	0
0.2	17.98	0.27
0.4	73.02	6.11
0.6	84.65	9.44
0.8	93.65	16.67
1.0	98.41	49.72
1.2	98.41	91.38
1.4	100	96.66
1.6	100	97.7
1.8	100	99.16
2.0	100	99.44
2.2	100	100
2.4	100	100

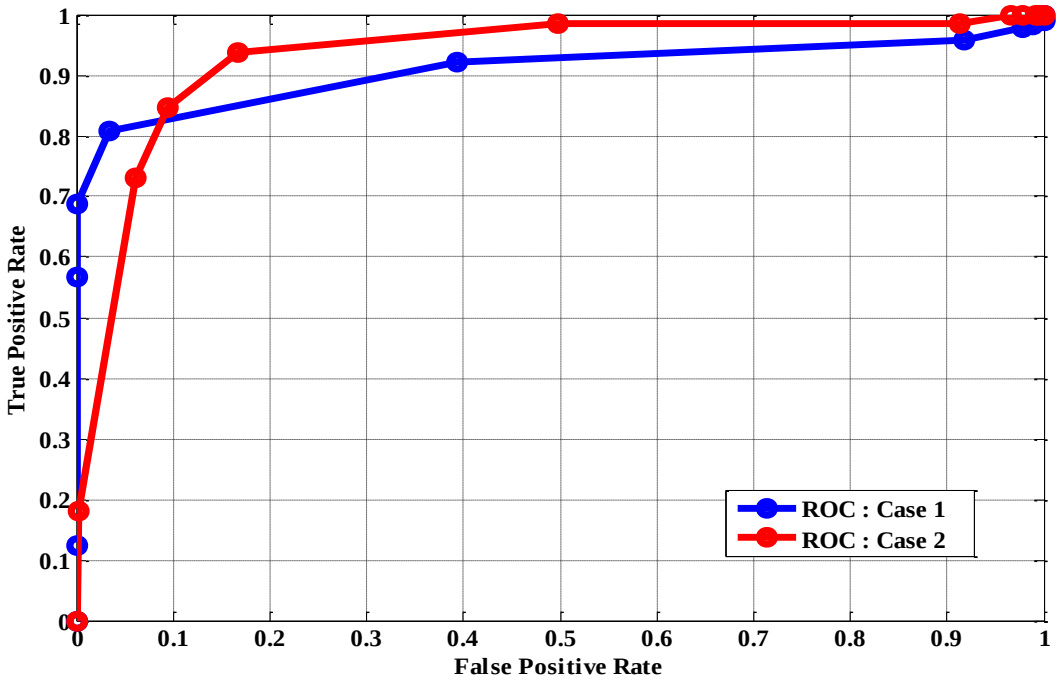

Figure 31. ROC curves for CZT peak amplitude.

4.5.8 ROC Analysis – Dominant DCT Coefficient

Table 10. ROC Table for Dominant DCT Coefficient

ROC Analysis: Case1

Threshold	TPR (%)	FPR (%)
0.0	0	0
0.2	20.56	0
0.4	50.35	0
0.6	67.37	0.74
0.8	79.07	8.9
1.0	90.42	43.07
1.2	95.03	78.65
1.4	96.45	91.76
1.6	98.22	97.37
1.8	98.58	98.87
2.0	98.93	99.25
2.2	99.64	100
2.4	99.64	100
2.6	100	100

ROC Analysis: Case2

Threshold	TPR (%)	FPR (%)
0.0	0	0
0.2	28.57	1.1
0.4	62.96	6.39
0.6	82.53	10
0.8	92.59	20
1.0	97.35	51.66
1.2	99.47	80.55
1.4	99.47	91.38
1.6	100	96.66
1.8	100	98.05
2.0	100	98.61
2.2	100	99.72
2.4	100	99.72
2.6	100	100

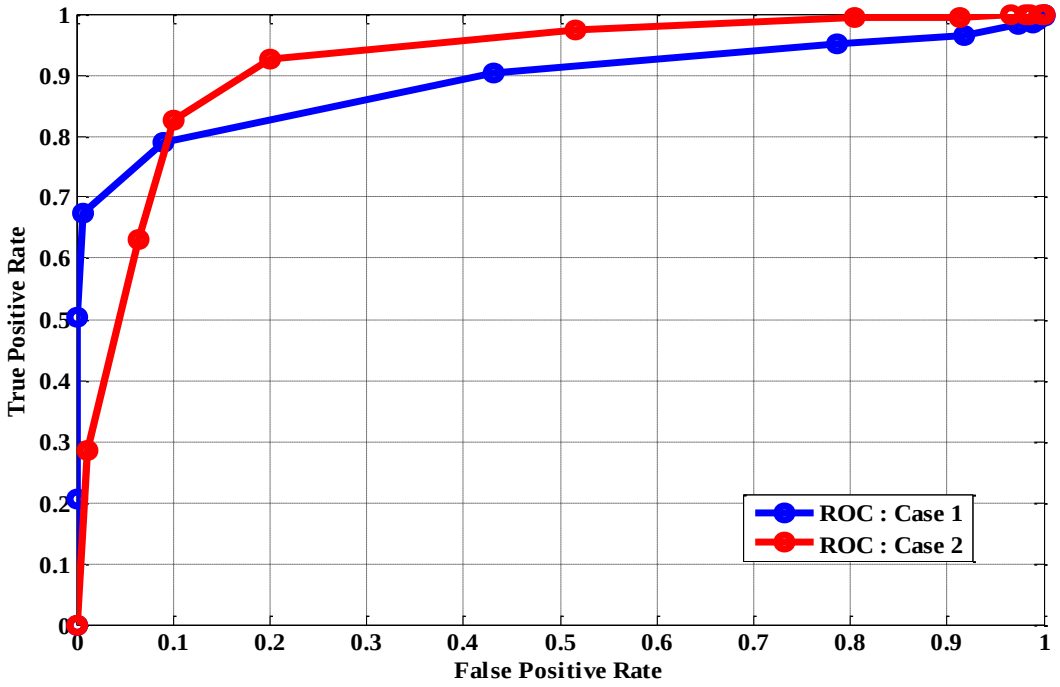

Figure 32. ROC curves for dominant DCT coefficient.

4.5.9 ROC Analysis – Dominant DST Coefficient

Table 11. ROC Table for Dominant DST Coefficient

ROC Analysis: Case1

Threshold	TPR (%)	FPR (%)
0.0	0	0
0.2	15.24	0
0.4	53.9	0
0.6	71.63	1.12
0.8	83.33	5.24
1.0	92.9	40.82
1.2	95.74	80.15
1.4	97.5	91.38
1.6	98.22	97
1.8	98.93	100
2.0	99.29	100
2.2	100	100
2.4	100	100

ROC Analysis: Case2

Threshold	TPR (%)	FPR (%)
0.0	0	0
0.2	22.2	0.28
0.4	69.31	5.83
0.6	87.83	10.83
0.8	97.35	18.05
1.0	100	50.55
1.2	100	81.94
1.4	100	91.66
1.6	100	96.38
1.8	100	99.16
2.0	100	99.44
2.2	100	100
2.4	100	100

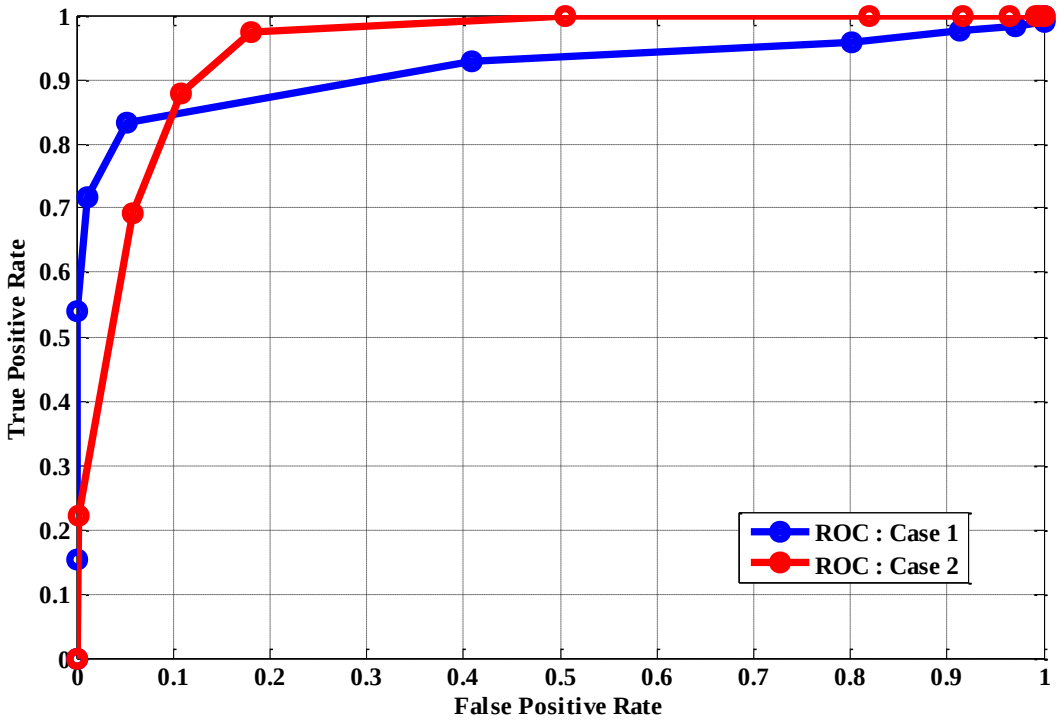

Figure 33. ROC curves for dominant DST coefficient.

4.6 LDA Performance Analysis for Yield Detection

The performance of our proposed LDA technique is also evaluated for the aforementioned two cases. Table 12 lists the true positive rates and the corresponding false positive rates. Figure 34 illustrates the respective ROC curves.

Table 12. ROC Table for LDA

ROC Analysis: Case1

Threshold	TPR (%)	FPR (%)
-0.3	0	0
-0.25	1.06	0
-0.2	35.81	0
-0.15	60.63	0
-0.1	80.14	0
-0.05	84.75	0
0	87.23	1.49
0.05	89.36	5.24
0.07	90.4	11.9
0.08	91.2	14.6
0.1	93.9	20.97
0.15	96.8	53.93
0.2	98.58	82.02
0.25	99.29	92.5
0.3	99.64	96.62
0.35	100	98.87
0.4	100	100

ROC Analysis: Case2

Threshold	TPR (%)	FPR (%)
-0.35	0	0
-0.33	9.5	0
-0.3	22.75	0.5
-0.28	32.27	1.3
-0.2	60.31	5.8
-0.15	79.8	6.9
-0.13	85.71	7.2
-0.1	91	8.8
-0.08	95.23	9.7
-0.05	98.41	10.83
-0.03	100	11.9
0.0	100	13.33
0.03	100	14.44
0.05	100	15.55
0.08	100	21.11
0.1	100	25.5
0.2	100	82.77
0.3	100	98.61
0.4	100	99.72
0.45	100	100

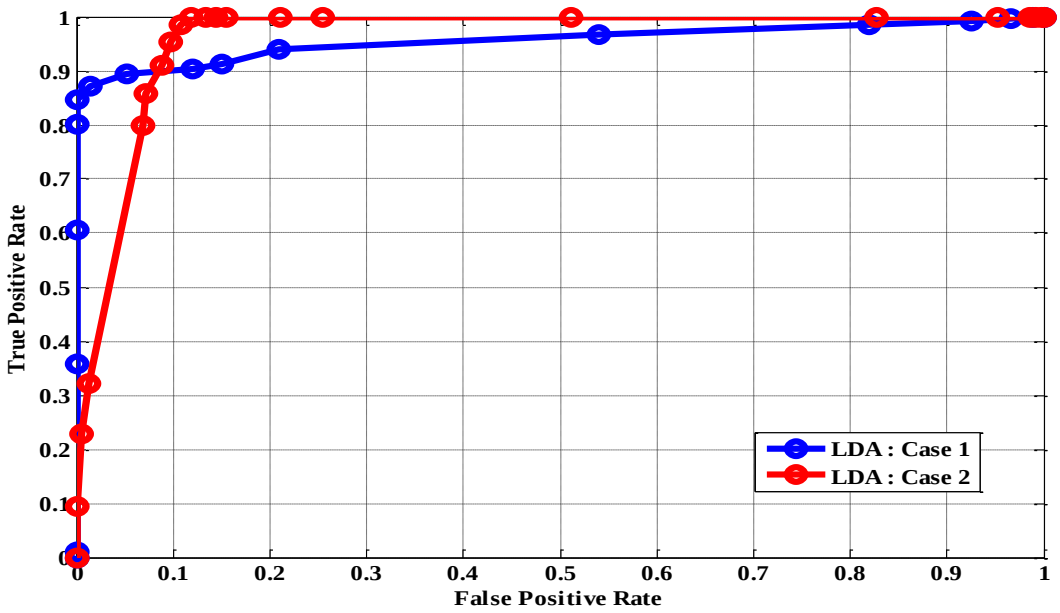

Figure 34. ROC curves for the LDA using all the above-mentioned signal features.

4.7 Performance Comparison of the Proposed LDA with Individual Signal Features

In the last section of this chapter, we demonstrate the comparisons based on the ROC curves between our proposed LDA technique and the conventional techniques using the aforementioned individual signal features. Figures 35 and 36 both illustrate the comparison of the nine signal features extracted from the ultrasonic echoes and the LDA technique integrating all these features for Case 1 while the former figure covers the range of false positive rate within [0, 1] but the latter figure covers the range of false positive rate within [0, 0.5] instead. Similarly, Figures 37 and 38 both illustrate the comparison of the nine signal features extracted from the ultrasonic echoes and the LDA technique integrating all these features for Case 2 while the former figure covers the range of false positive rate within [0, 1] but the latter figure covers the range of false positive rate within [0, 0.55] instead.

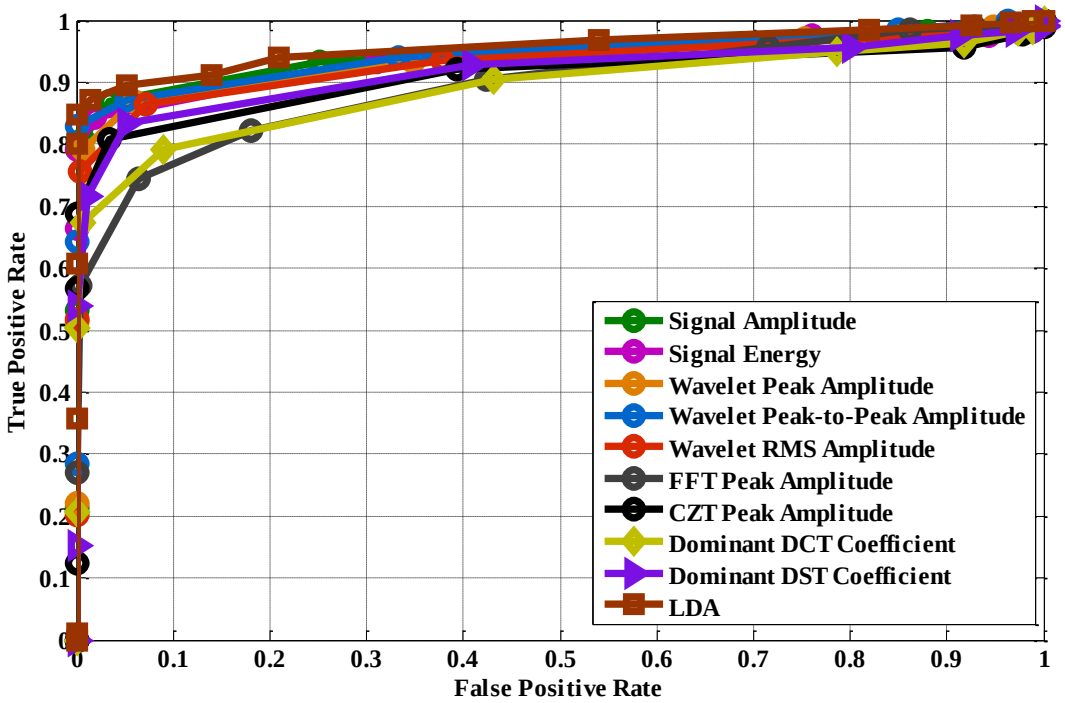

Figure 35. ROC curves for Case 1 (the range of false positive rate is [0, 1]).

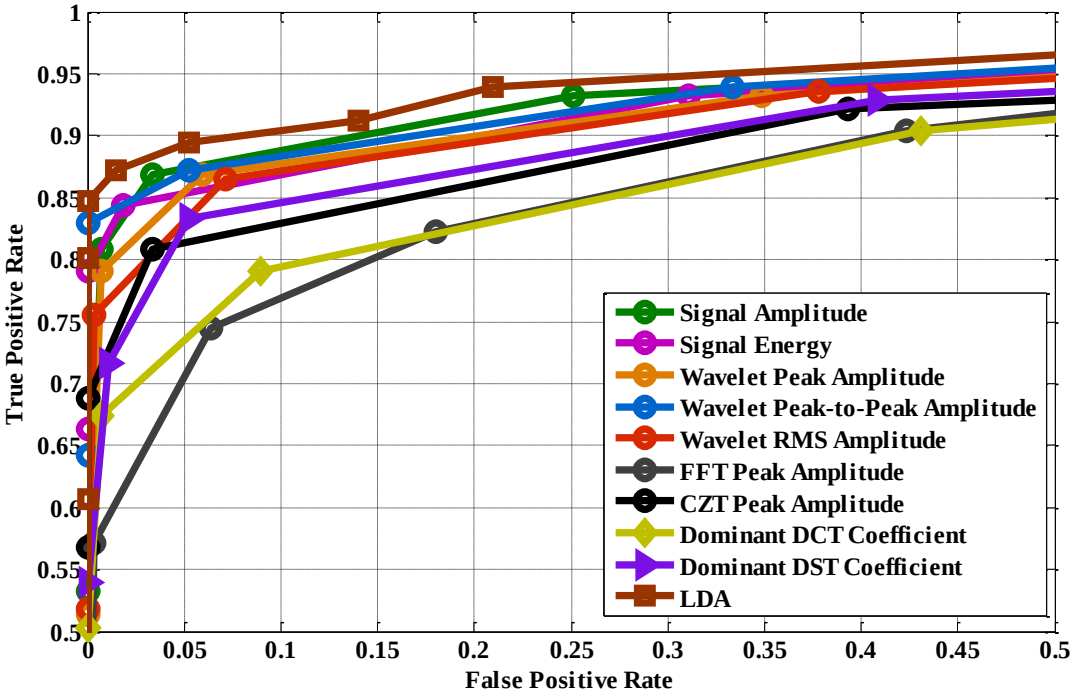

Figure 36. ROC curves for Case 1 (the range of false positive rate is [0, 0.5]).

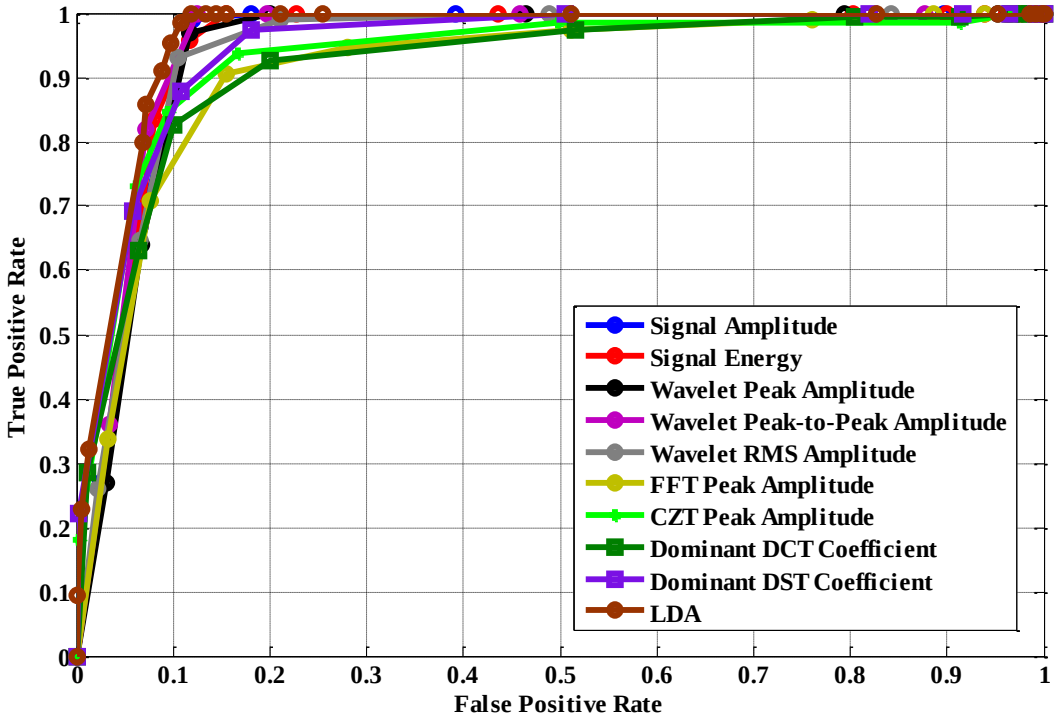

Figure 37. ROC curves for Case 2 (the range of false positive rate is [0, 1]).

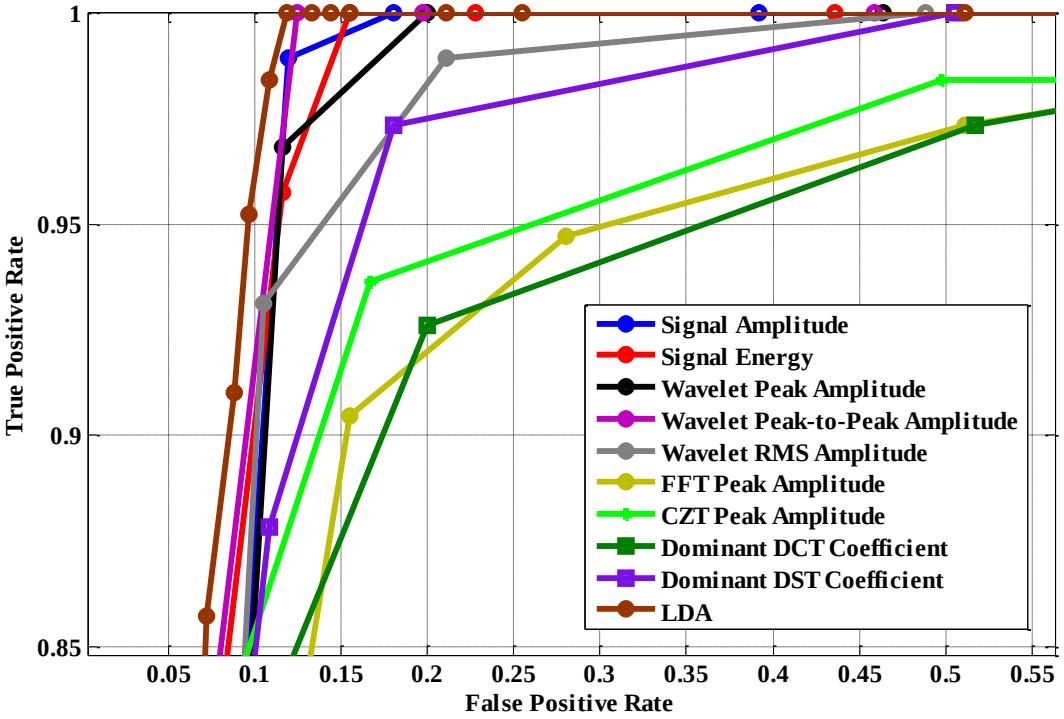

Figure 38. ROC curves for Case 2 (the range of false positive rate is [0, 0.55]).

Table 13, lists the true positive rates (TPRs) for the nine signal features and the LDA technique for Case 1 subject to a fixed false positive rate of 10%, which can be considered a practically allowable false alarm rate.

Table 13. True Positive Rate Comparison Subject to 10% of False Positive Rate

Features	TPR
Signal Amplitude	87%
Signal Energy	88%
Wavelet Peak Amplitude	86%
Wavelet Peak-to-Peak Amplitude	88%
Wavelet RMS Amplitude	87%
FFT Peak Amplitude	77%
CZT Peak Amplitude	83%
Dominant DCT Coefficient	79%
Dominant DST Coefficient	84%
LDA	92%

According to Table 13, our proposed LDA technique is “optimal” among all. Besides, according to Figures 35-38, it can be observed that for almost all false positive rates, our proposed LDA achieves the highest true positive rates among all techniques in comparison.

CHAPTER 5: CONCLUSION

In this thesis, a novel NDT tool for yield detection using ultrasonic signal features is proposed and studied. The obtained ultrasonic signal waveforms for the Type-I steel specimens are sampled and investigated for the yield analysis. The ultrasonic signals are preprocessed and segmented and a total of three dominant echoes from each waveform are extracted.

Both time-domain features (peak amplitude, signal energy) and transform-domain features (wavelet peak amplitude, wavelet peak-to-peak amplitude, wavelet RMS amplitude, FFT peak amplitude, CZT peak amplitude, dominant DCT coefficient, dominant DST coefficient) are extracted from the three dominant echoes. After the extraction of the features, the graphic analysis and the statistical analysis are carried out for every signal feature to observe the corresponding separability to distinguish yield and no-yield conditions.

We also propose an integrative framework built upon the linear discriminant analysis (LDA) to further improve the yield detection method using either of the nine individual signal features in the time- and transform-domains. The receiver-operating-characteristics (ROC) curves are depicted to compare different features. From our experiments, we have discovered that the proposed LDA technique leads to the best ROC results for yield detection.

REFERENCES

[1] C. R. Farrar and K. Worden, "An introduction to structural health monitoring," *Philosophical Transcations of the Royal Society A*, vol. 365, pp. 303-315, February 2007.

[2] M. Krüger, C. U. Grosse, and P. J. Marrón, "Wireless structural health monitoring using MEMS," *Key Engineering Materials*, vol. 293-294, pp. 625-634, 2005.

[3] NDT Resource Center. [Online]. http://www.ndt-ed.org/AboutNDT/aboutndt.htm

[4] G. P. Singh and S.Udpa, "The role of digital signal processing in NDT," *NDT International*, vol. 19, no. 3, pp. 125-132, June 1986.

[5] H. Toutanji, "Ultrasonic wave velocity signal interpretation of simulated concrete bridge decks," *Materials and Structures/Materiaux et Constructins*, vol. 33, no. 227, pp. 207-215, April 2000.

[6] M. Berke, "Non destructive material testing with ultrasonics-intoduction to the basic principles," [Online] http://www.ndt.net/article/v05n09/berke/berke1.htm, vol 5, no. 9, September 2000.

[7] H.-C. Wu, N. Gupta, and P. S. Mylavarapu, "Blind multiridge detection for automatic nondestructive testing using ultrasonic signals," *IEEE Transactions on Ultrasonics, Ferroelectrics and Frequency Control*, vol. 53, no. 10, pp. 1902-1911, October 2006.

[8] "The American Society for Non Destructive Testng". [Online]. http://www.asnt.org/ndt/primer2.htm

[9] NDT Resource Center. [Online]. http://www.ndt-ed.org/EducationResources/CommunityCollege/Ultrasonics/Introduction/history.htm

[10] A. M. Okeil and Y. Bingol, "Ultrasonic signal characteristics in pre- and post-yield steel structures ," *Electronic Journal Of Structural Engineering*, vol. 9, pp. 1-9, 2009.

[11] E. Schneider. "Nondestructive analysis of stress states in components using micromagnetic and ultrasonic techniques," [Online] http://www.ndt.net/article/ecndt98/material/139/139.htm vol 3, no. 11, November 1998.

[12] A. N. Guz and F. G. Makhort, "The physical fundamentals of the ultrasonic nondestructive stress analysis of solids," *International Applied Mechanics*, vol. 36, no. 9, pp. 1119-1149, 2000.

[13] Y. Bingol and A. M. Okeil, "Yield detection in steel structures using ultrasonic pulse signals," *Transportation Research Board 87th Annual Meeting*, 2008.

[14] S. W. Smith, *The Scientist and Engineers Guide to Digital Signal Processing*, 1st ed., 1997.

[15] "Katja's Home Page on Sinusoids, complex numbers and modulation". [Online]. http://www.katjaas.nl/chirpZ/chirpZ.html

[16] L. B. Rabiner, R. W. Schafer, and C. M. Rader, "The chirp *z*-transform algorithm," *IEEE Transactions on Audio and Electroacoustics*, vol. AU-17, no. 2, pp. 86-92, June 1969.

[17] G. D. Martin, *Chirp Z-Transform Spectral Zoom Optimization Using MATLAB*, Technical Report, Sandia National Laboratories, 2005.

[18] K. Ravali, P. A. Kumar, and S. Asadi, "Carrying digital watermarking for medical imgaes using mobile devices," *Internation Journal of Computer Science and Engineering Technology*, vol. 1, no. 7, pp. 366-369, August 2011.

[19] K. R. Rao and P. C. Yip, *The Transform and Data Compression Handbook*, CRC Press, 2000.

[20] N. Ahmed, T. Natarajan and K. R. Rao, "Discrete cosine transform," *IEEE Transactions on Computers*, vol. C-23, no. 1, pp. 90-93, January 1974.

[21] Mathworks. DCT Documentation. [Online]. www.mathworks.com/help/signal/ref/dct.html 2010.

[22] V. Britanak, K. R. Rao, and P. C. Yip, *The Transform and Data Compression Handbook*, CRC Press, 2001.

[23] Mathworks. DST, IDST Documentation. [Online]. www.mathworks.com/help/pde/ug/idst.html , 2010.

[24] A. K. Jain, "A sinusoidal family of unitary transforms," *IEEE Transactions on Pattern Analysis and Machine Intelligence* , vol. PAMI-1, no. 4, pp. 356-365, October 1979.

[25] A. M. Martinez and A. C. Kak, "PCA versus LDA," *IEEE Transcations on Pattern Analysis and Machine Intelligence*, vol. 23, no. 2, pp. 228-233, February 2001.

[26] R. A. Fisher, "The use of multiple measures in taxonomic problems ," *Ann Eugenics*, vol. 7, pp. 177-188, 1936.

[27] A. Sadr and S. Ehteram, "Intelligent MFL defect detection algorithm equipped by linear discriminant analysis," *The E-Journal of Non-Destructive Testing*, May 2008.

[28] A. A.Rosario, L. R. Padovese, R. Medina-Aguas and C. P. Serna-Giraldo, "Principal

component analysis and discriminant analysis as a supervised pattern recognition tool for classification of AISI 420 steel samples subjected to a different heat treatment using magnetic Barkhausen noise signals," in *Proceedings of 18th World Conference on Non destructive Testing*, Durban, South Africa, April 2012.

[29] R. Polikar, "The engineers ultimate guide to wavelet analysis," [Online], http://users.rowan.edu/~polikar/WAVELETS/WTtutorial.html, January 2001.

VITA

Bharath Murali Thekkedath was born in 1987 in Trichur, in the state of Kerala, India. He did his schooling in Hyderabad and graduated in Bachelors of Engineering from Anna University, Chennai. After his graduation in 2008, he later joined the Department of Electrical Engineering at LSU in Fall 2009 and will be graduating in May 2013.